Chapter 4
Pulse Doppler Radar*

John P. Stralka
William G. Fedarko

Northrop Grumman Corporation

4.1 CHARACTERISTICS AND APPLICATIONS

The primary benefit of pulse doppler radar is its ability to detect small-amplitude moving target returns against an overwhelmingly large-amplitude clutter background.

Nomenclature. Radars that rely on the doppler effect to enhance target detection are called *doppler radars*.[1] The doppler effect manifests itself when there is a relative range rate, or radial velocity, between the radar and the target. When the radar's transmit signal is reflected from such a target, the carrier frequency of the return signal will be shifted. Assuming a monostatic radar (i.e., collocated transmitter and receiver), the roundtrip distance is twice the distance between the transmitter and the target. The doppler frequency shift f_d is a function of the carrier wavelength λ and the relative radial velocity (range rate) between the radar and the target V_{relative}, and is written as $f_d = -2V_{\text{relative}}/\lambda$, where $\lambda = c/f$ is the wavelength, c is the speed of light, and f is the carrier frequency. When the target is moving away from the radar, the relative radial velocity, or range rate, is defined to be positive and results in a negative doppler shift.

Doppler radars can be either continuous wave (CW)† or pulsed radars. CW radars simply observe the doppler shift between the carrier frequency of the return signal relative to the transmit signal. Pulsed systems measure doppler by using a coherent train of pulses where there is a fixed or deterministic phase relationship of the carrier frequency between each successive radio frequency (RF) pulse. Coherence concentrates the energy in the frequency spectrum of the pulse train around distinct spectral lines, separated by the pulse repetition frequency (PRF). This separation into spectral lines allows for discrimination of doppler shifts.

Doppler radars using pulsed transmissions are more complex than CW radars, but they offer significant advantages. Most important is the time gating of the receiver.

* David H. Mooney and William A. Skillman wrote this chapter for the first edition (1970). William H. Long joined the authors for the second edition (1990). John P. Stralka and William G. Fedarko updated the material for this edition.

† To assist the reader, abbreviations used throughout this chapter are defined in a list at the end of the chapter.

Time gating allows the blanking of direct transmitter leakage into the receiver. This permits the use of a single antenna for transmit and receive, which otherwise would not be feasible for CW radar due to excessive transmit/receive isolation requirements. Pulsed radars can also use range gating, a specific form of time gating, which divides the interpulse period into cells or *range gates*. The duration of each cell is typically less than or equal to the inverse of the transmit pulse bandwidth. Range gating helps eliminate excess receiver noise from competing with target returns and allows range measurement with pulse delay ranging (i.e., measuring the time between transmission of a pulse and reception of the target echo).

Pulsed transmission doppler radars have historically been categorized as *moving target indication (MTI)* or *pulse doppler*. MTI typically eliminates clutter by passing the received returns from multiple coherent pulses through a filter with a stopband placed in spectral regions of heavy clutter concentrations. Moving targets with doppler frequencies outside the stopband are passed onto detection processing. Pulse doppler radars, on the other hand, resolve and enhance targets within a particular doppler band while rejecting clutter and other returns outside the doppler band of interest. This is typically accomplished with a contiguous bank of doppler filters formed between two of the coherent pulse train's spectral lines, one of which is the central line. Range gating precedes the doppler filter bank. The bandwidth of each doppler filter is inversely proportional to the duration of the coherent pulse train that is processed to form the doppler filter bank. This process forms a matched filter to the entire pulse train.[2,3]

MTI and pulse doppler radars share the following characteristics:

- Coherent transmission and reception; that is, each transmitted pulse and the receiver local oscillator are synchronized to a free-running, highly stable oscillator.
- Coherent processing to reject main-beam clutter, enhance target detection, and aid in target discrimination or classification.

MTI radars can also be implemented using a doppler filter bank, blurring the historic delineation between MTI and pulse doppler radars. As a result, this book will define MTI radars as those radars whose PRF is sufficiently low enough to provide an unambiguous range measurement, via pulse delay ranging, over the radar's instrumented range. The unambiguous range R_u is given by $c/(2f_R)$, where c is the speed of light and f_R is the PRF. Radars with PRFs that result in range ambiguities within the range coverage of interest will be referred to as pulse doppler radars and will be the focus of this chapter.

Applications. Pulse doppler is applied principally to radar systems requiring the detection of moving targets in a severe clutter environment. Table 4.1 lists typical applications and requirements.[4–12] This chapter will deal principally with airborne applications, although the basic principles can also be applied to the surface-based case. Only monostatic radars will be considered.

PRFs. Pulsed radars that employ doppler are divided into three broad PRF categories: low, medium, and high. A low-PRF radar is one in which the ranges of interest are unambiguous while the radial velocities (doppler frequencies) are usually highly ambiguous. As discussed previously, this type of radar is called *moving target indication (MTI)*. MTI radars are generally not categorized as pulse doppler radars, although the principles of operation are similar.[13]

TABLE 4.1 Pulse-Doppler Applications and Requirements

Radar Application	Requirements
Airborne or spaceborne surveillance	Long detection range; accurate range data
Airborne interceptor or fire control	Medium detection range; accurate range, velocity, and angle data
Ground-based surveillance	Medium detection range; accurate range data
Battlefield surveillance (slow-moving target detection)	Medium detection range; accurate range, velocity data
Missile seeker	Short detection range; accurate velocity and angle rate data; may not need true range information
Surface-based weapon control	Short range; accurate range, velocity data
Meteorological	Good velocity resolution
Missile warning	Short detection range; very low false-alarm rate

The converse of a low-PRF radar is a high-PRF radar that can measure doppler unambiguously over the span of radial velocities of interest, but is usually highly ambiguous in range. A medium-PRF radar has both range and doppler ambiguities.[14–17] A blend of medium and high PRF, known as high-medium PRF (which will be discussed later), is characterized as having only a single-ambiguity for the radial velocities of interest. For this chapter, a pulse doppler radar is characterized as having a PRF anywhere within the medium to high PRF regime that results in ambiguous range measurements during a coherent processing interval.

A comparison of MTI and pulse doppler radars is shown in Table 4.2. Previously undefined terms will be defined throughout the chapter. The table assumes an airborne radar application designed to detect other aircraft. Such an application is commonly referred to as *air-to-air*.

TABLE 4.2 Comparison of MTI and Pulse Doppler Radars for Air-to-Air

	Advantages	Disadvantages
Low PRF *MTI* range unambiguous doppler ambiguous	Can sort clutter from targets on basis of range. Front-end sensitivity time control (STC) suppresses sidelobe detections at short ranges and reduces dynamic range requirements.	Multiple blind speeds. Usually does not measure radial target velocity. Poor ground-moving target rejection.
Medium PRF *Pulse Doppler* range ambiguous doppler ambiguous	Performance at all target aspects. Good ground-moving target rejection. Measures radial velocity. Less range eclipsing than in high-PRF.	Sidelobe clutter can limit performance. Ambiguity resolution required. Low antenna sidelobes necessary. Rejection of sidelobe returns of discrete ground targets needed.
High PRF *Pulse Doppler* range ambiguous doppler unambiguous	Allows thermal noise-limited detection of targets with high radial velocities. Single doppler blind zone at zero velocity. Good ground-moving target rejection. Measures radial velocity.	Limited low radial velocity target detection. Range eclipsing. Large number of range ambiguities preclude pulse delay ranging. High stability requirements due to range folding.

TABLE 4.3 Typical Values for an X-band (10 GHz) Airborne Fire-Control Radar

Pulse Doppler Waveform	PRF	Transmit Duty Cycle
Medium PRF	10–40 kHz	5–10%
High-medium PRF	60–100 kHz	10–20%
High PRF	120–300 kHz	15–50%

Table 4.3 provides the span of PRFs and corresponding transmit *duty cycles* (ratio of transmit pulse width to interpulse period) for the various pulse doppler waveforms used in a X-band airborne fire-control radar. Keep in mind that the operating frequency of the radar, along with its required range and radial velocity coverage, determines whether a PRF is considered medium, high-medium, or high. Also, modern multifunction radars are typically capable of utilizing waveforms from the various PRF categories in order to carry out their diverse missions.

Pulse Doppler Spectrum. The transmitted spectrum of a pulse doppler radar consists of discrete lines at the carrier frequency f_0 and at sideband frequencies $f_0 \pm if_R$, where f_R is the PRF and i is an integer. The envelope of the spectrum is determined by the pulse shape. For the rectangular pulses usually employed, a $\sin(x)/x$ spectrum is obtained.

Using a constant-velocity airborne radar, the received spectrum from a stationary target has lines that are doppler-shifted proportionally to the radial velocity between the radar platform and the target. The two-way doppler shift is given by $f_d = (2V_R/\lambda)\cos(\psi_0)$, where λ is the radar wavelength, V_R is the radar platform speed, and ψ_0 is the angle between the velocity vector and the line of sight to the target. (Note that the relative radial velocity (range rate) to the stationary target is $V_{\text{relative}} = -V_R\cos(\psi_0)$, which makes the later equation for doppler shift consistent with the one presented at the beginning of the chapter.) Illustrated in Figure 4.1 is the received pulsed spectrum with returns from distributed clutter, such as the ground or weather, and from discrete targets, such as aircraft, automobiles, tanks, etc.

Figure 4.2 shows the unfolded spectrum (i.e., no spectral foldover from adjacent PRF lines) in the case of horizontal motion of the radar platform, with a speed V_R. The clutter-free region is defined as that portion of the spectrum in which no ground clutter can exist. (A clutter-free region usually does not exist with medium PRFs due to doppler folding.) The sidelobe clutter region, $4V_R/\lambda$ in width, contains ground clutter power from the sidelobes of the antenna, although this clutter power may be below the noise level in part of the region. The main-beam clutter region, located at $f_0 + (2V_R/\lambda)\cos(\psi_0)$, contains the strong return from the main beam of the antenna

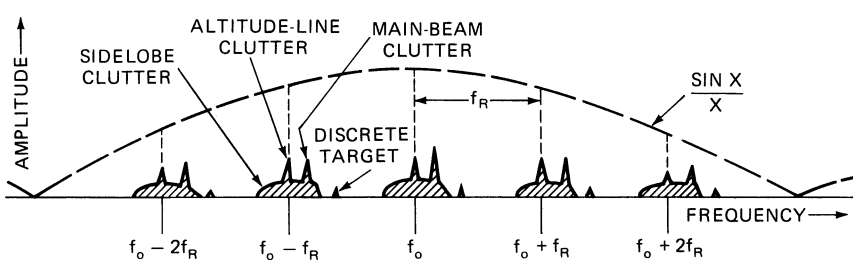

FIGURE 4.1 Clutter and target frequency spectrum from a horizontally moving platform

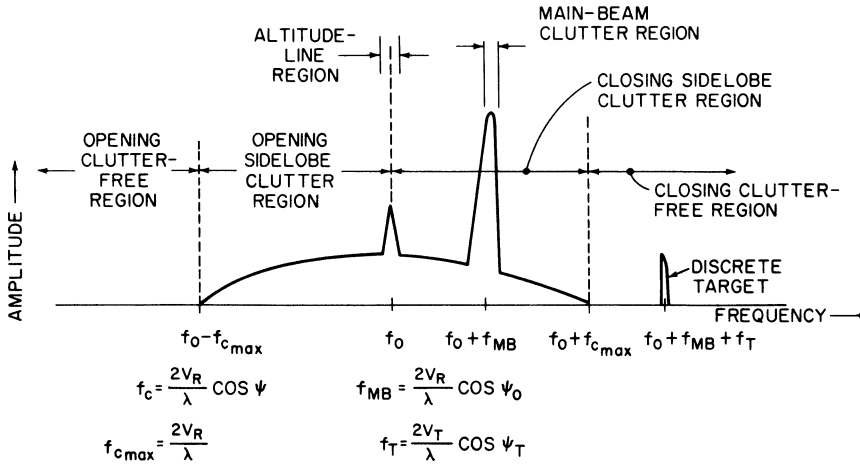

FIGURE 4.2 Unfolded spectrum (with no clutter positioning)

striking the ground at a scan angle of ψ_0, measured from the velocity vector. Rain and chaff clutter may also be large when the main beam illuminates a rain or chaff cloud. Motion due to winds may displace and/or spread the return in frequency.

Altitude-line clutter is due to the radar return from ground clutter at near normal incidence directly below the radar platform, and is at zero doppler if there is no vertical component of platform velocity. A discrete target return in the main beam is shown at $f_T = f_0 + (2V_R/\lambda)\cos(\psi_0) + (2V_T/\lambda)\cos(\psi_T)$, where the target speed is V_T, with an angle ψ_T between the target velocity vector and the radar target line of sight. The components of the spectrum shown in Figure 4.2 will also vary with range, as discussed later. (Note that the direction of $V_T\cos(\psi_T)$ is assumed to be the opposite of $V_R\cos(\psi_0)$ resulting in a relative range rate of $V_{\text{relative}} = -V_T\cos(\psi_T) - V_R\cos(\psi_0)$, which is consistent with the definition for doppler shift stated at the beginning of the chapter.)

Figure 4.3 illustrates the various clutter doppler frequency regions as a function of the antenna main-beam azimuth and relative radar and target velocities, again for an unfolded spectrum. The ordinate is the radial or line-of-sight component of target velocity in units of radar platform velocity, so the main-beam clutter region is at zero velocity and the sidelobe clutter region frequency boundaries vary sinusoidally with antenna azimuth. Thus, the figure shows the doppler regions in which the target becomes clear of sidelobe clutter. For example, if the antenna main-beam azimuth angle is at zero, any head-on target ($V_T\cos(\psi_T) > 0$) is clear of sidelobe clutter, whereas if the radar is in trail behind the target ($\psi_T = 180°$ and $\psi_0 = 0°$), the target's radial velocity has to be greater than twice that of the radar to become clear of sidelobe clutter.

The sidelobe clear and clutter regions can also be expressed in terms of the aspect angle with respect to the target, as shown in Figure 4.4.[18] Here, collision geometry is assumed in which the radar and target aircraft fly straight-line paths toward an intercept point; the look angle of the radar ψ_0 and the aspect angle of the target ψ_T are constant for a given set of radar and target speeds V_R and V_T, respectively. The center of the diagram is the target, and the angle to the radar on the circumference is the aspect angle. The aspect angle and look angles satisfy the equation $V_R \sin(\psi_0) = V_T \sin(\psi_T)$,

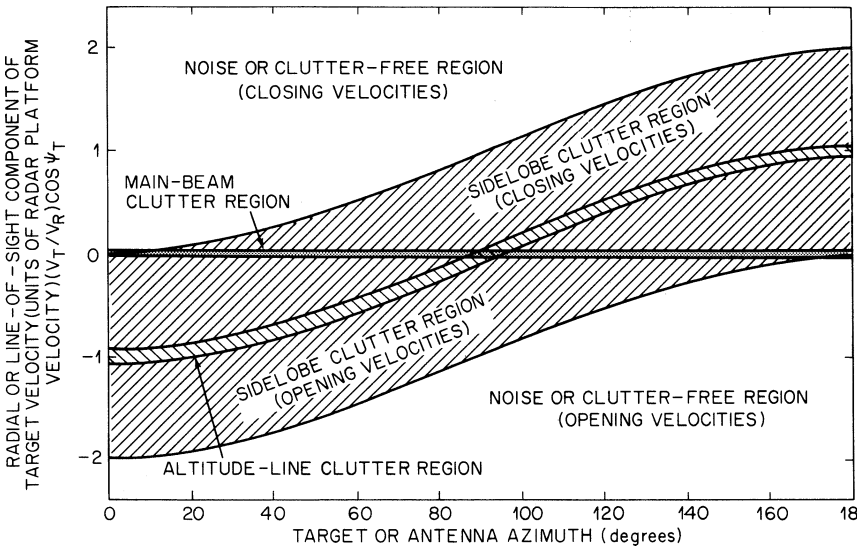

NOTE: Width of altitude-line and main-beam clutter regions varies with conditions; azimuth is measured from radar platform velocity vector to the antenna boresight or to the line of sight to the target; horizontal-motion case.

FIGURE 4.3 Clutter and clutter-free regions as a function of target velocity and azimuth

which is defined as a collision course. The target aspect angle is zero for a head-on condition and 180° for a tail chase. The aspect angle corresponding to the boundary between the sidelobe clutter region and the sidelobe clear region is a function of the relative radar-target velocity ratio and is shown in Figure 4.4 for four cases. Case 1 is where the radar and target speeds are equal and the target can be seen clear of sidelobe clutter in a head-on aspect out to 60° on either side of the target's velocity vector. Similarly, Cases 2 through 4 show conditions where the target's speed is 0.8, 0.6, and 0.4 times the radar's speed, in which case the target can be seen clear of sidelobe clutter over a region of up to ±78.5° relative to the target's velocity vector. Again, these conditions are for an assumed collision course. As is evident, the aspect angle of the target clear of sidelobe clutter is always forward of the beam aspect.

Ambiguities and PRF Selection. Pulse doppler radars are ambiguous in range and possibly doppler. As mentioned earlier, the unambiguous range R_u is given by $c/(2f_R)$, where c is the speed of light and f_R is the PRF.

If the airborne target radial velocity to be observed is between $V_{T,\max,\text{opening}}$ for opening targets (positive range rate) and $-V_{T,\max,\text{closing}}$ for closing targets (negative range rate), then the minimum value of PRF, $f_{R\,\min}$, which is unambiguous in velocity (in both magnitude and sense, i.e., positive and negative), is

$$f_{R,\min} = 2(V_{T,\max,\text{closing}} + V_{T,\max,\text{opening}} + V_g)/\lambda \tag{4.1}$$

where V_g is the upper limit for ground moving target rejection. V refers to the speed, or the magnitude of the range rate.

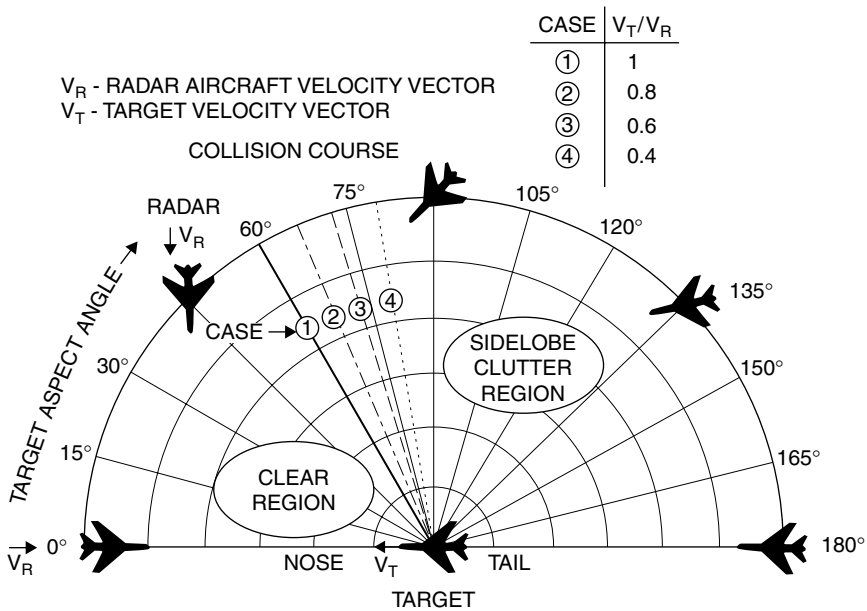

FIGURE 4.4 Sidelobe clutter-clear regions versus target aspect angle. Note the target is at the center of the plot with the radar platform on the circumference.

However, some pulse doppler radars employ a PRF that is unambiguous in velocity magnitude only, i.e., $f_{R,\min} = 2\,[\max(V_{T,\max,\text{closing}}, V_{T,\max,\text{opening}}) + V_g]/\lambda$, and rely on detections in multiple PRFs during the time on target to resolve the sign ambiguity in doppler. These radars can be described as *high-medium*-PRF and can be considered to be in the high-PRF category if the older definition of high PRF (no velocity ambiguity) is extended to allow one velocity ambiguity, that of doppler sense. The lower PRF eases the measurement of true range while retaining the high-PRF advantage of a single blind-speed region near zero doppler. High-medium PRF is becoming more prevalent in modern airborne radars for air-to-air search.

The choice between high and medium PRF involves a number of considerations, such as transmitter duty cycle limit, pulse compression availability, signal-processing capability, measurement accuracy requirements, etc., but often depends on the need for all-aspect target detectability. All-aspect coverage requires good performance in tail chase, where the target doppler is in the sidelobe clutter region near the altitude-line. In a high-PRF radar, the range foldover may leave little clear region in the range dimension, thus degrading target detectability. By using a lower or medium PRF, the clear region in range is increased at the expense of velocity foldover for high-doppler targets that are in the clutter-free region in high PRF. As an example, Figure 4.5 shows the clutter-plus-noise-to-noise ratio in range-doppler coordinates for two different X-band waveforms at similar altitudes and aircraft velocities. The range dimension represents the unambiguous range interval R_u, and the frequency dimension represents the PRF interval, with the main-beam clutter, altitude-line, and sidelobe clutter regions clearly discernible. In both waveforms, the main-beam clutter return is positioned to DC through clutter positioning via an

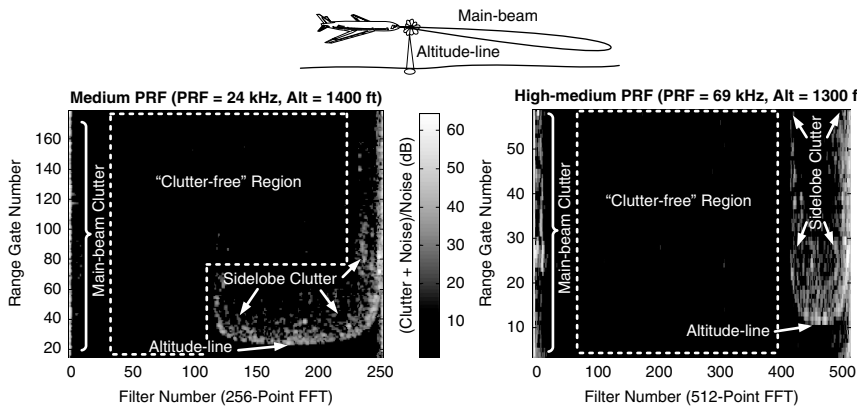

FIGURE 4.5 Clutter-plus-noise-to-noise ratio in range-doppler space

offset applied to the transmit frequency. The medium-PRF spectrum (PRF = 24 kHz) contains a range-doppler region in which the sidelobe clutter is below thermal noise and in which good tail-aspect target detectability can be achieved. The 69 kHz high-medium PRF waveform has a much more severe clutter folding, and tail aspect targets would compete with sidelobe clutter at nearly all ranges, but the clutter-free region is much larger.

Because the clutter is folded in both range and doppler with medium-PRF, a number of PRFs may be required to obtain a satisfactory probability of sufficient detections to resolve the range and doppler ambiguities. The multiple PRFs move the relative location of the clear regions so that all-aspect target coverage is achieved. Since the sidelobe clutter generally covers the doppler region of interest, the ratio of the region with sidelobe clutter below noise relative to the total range-doppler space is a function of the radar altitude, speed, and antenna sidelobe level.

If a high-PRF waveform is used, the clear-range region disappears because the sidelobe clutter folds in range into the unambiguous range interval (assuming the target doppler is such that it still competes with the sidelobe clutter). However, in those doppler regions free of sidelobe clutter, as shown in Figure 4.3 and Figure 4.4, target detectability is limited only by thermal noise, independent of radar altitude, speed, and sidelobe level. This requires system stability sidebands to be well below noise for the worst-case main-beam clutter. Thus, although medium PRF provides all-aspect target coverage, the target is potentially competing with sidelobe clutter at all aspects, whereas with high PRF, a target can become clear of sidelobe clutter at aspect angles forward of the beam aspect.

For targets with sufficient radial velocity, high PRF is typically more efficient than medium PRF. The transmit pulse width is usually limited by the transmitter's ability to preserve the pulse amplitude and phase characteristics over the duration of the transmit pulse. For a fixed transmit pulse width and peak power, a waveform with a higher PRF will have a higher transmit duty cycle resulting in a higher average transmit power. For a given coherent processing time, more energy is placed on the target, which improves detectability. For this reason, high PRF is used for long-range search of high-speed closing targets.

Range Gating. Range gating divides the time between transmit pulses into multiple cells or range gates. Range gating eliminates excess receiver noise and clutter from competing with the signal and permits target tracking and range measurement. The range gate is typically matched to the bandwidth of the transmit pulse. In a surveillance radar, a number of receiver gates are used to detect targets that may appear at any range within the interpulse period. Figure 4.6 illustrates the general case where the gate spacing τ_s, the gate width τ_g, and the transmitted pulse τ_t are all unequal. Selecting $\tau_t = \tau_g$ maximizes target return signal-to-noise ratio and, as a result, range performance. Selecting $\tau_g > \tau_s$ creates overlapped range gates and reduces the range gate straddle loss (Section 4.6) but can increase the possibility of range ghosts unless contiguous detections from straddled target returns are "clumped" prior to the ambiguity resolution (Section 4.4). With range gating, the range measurement accuracy is on the order of the range gate size (150 m/μs), but this can be improved to a fraction of the gate width by amplitude centroiding.

Timeline Definitions. Pulse doppler radar works on several different time scales. Various organizations have their own nomenclature for time-based parameters. Therefore, the timeline definitions used throughout this chapter are defined here.

Figure 4.7 illustrates the different time scales. Starting at the lowest level, a series of coherent pulses are transmitted at a pulse repetition frequency (PRF). The time between the pulses is the *interpulse period* (IPP), which is simply the inverse of the PRF. The receive portion of the IPP is broken up into range gates. The *transmit duty cycle* is the transmit pulse width divided by the IPP. The train of pulses is called the *coherent processing interval* (CPI). The coherent processing forms a bank of doppler

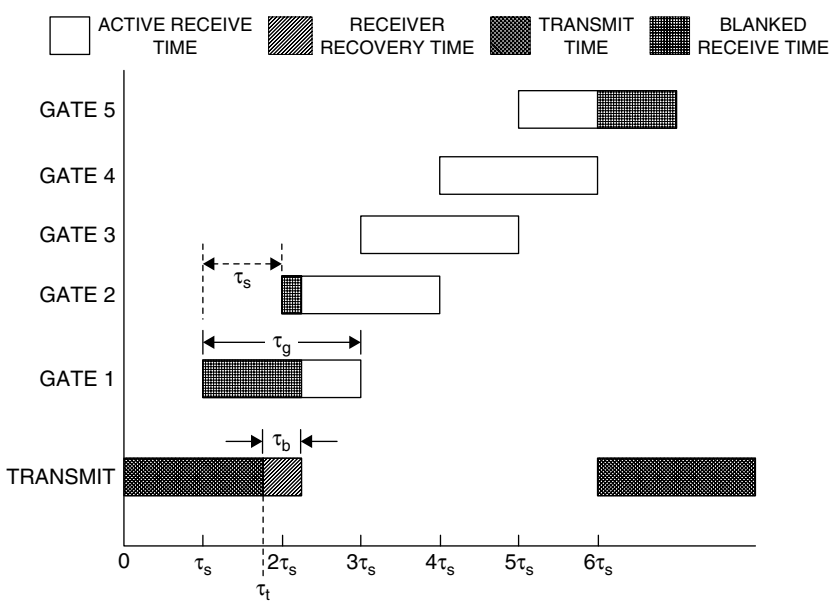

FIGURE 4.6 Example of range gates with 50% overlap equally spaced in the interpulse period. τ_b represents the extra blanking time after the transmit pulse to allow for receiver/protector recovery.

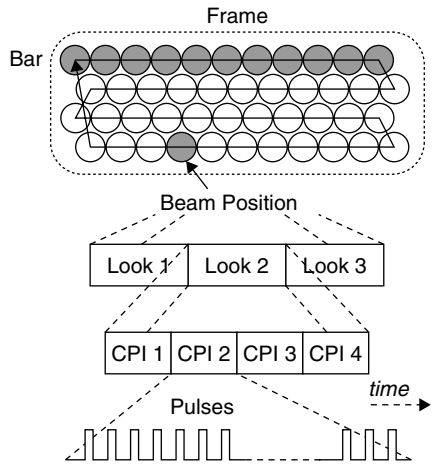

FIGURE 4.7 Pulse doppler dwell timeline

filters for each range gate resulting in a range-doppler map for a CPI, similar to that shown in Figure 4.5.

Several CPIs with the same PRF, but possibly different transmit carrier frequencies, can be noncoherently combined via *postdetection integration* (PDI). If frequency modulation (FM) ranging is used, all the CPIs that are noncoherently integrated must have the same FM slope. The grouping of CPIs is a *look*. Detections are determined for the range-doppler cells in a look.

Multiple looks with different PRFs or frequency modulations are used to resolve range and/or doppler ambiguities. This group of looks is a dwell. A dwell is associated with a particular antenna line-of-sight or *beam position*. Target reports are generated for each dwell.

A *bar* refers to a line of beam positions at a constant elevation. In search, a multibar *raster* scans the beam over an assigned area or volume to create a *frame*. A frame may have multiple bars. Typically, the antenna will visit every beam position once during a search frame.

Basic Configuration. Figure 4.8 shows a representative configuration of a pulse doppler radar utilizing digital signal processing under the control of a mission processor. Included are the antenna, receiver/exciter, signal processor, and data processor. The radar's control processor receives inputs from the on-board systems, such as the inertial navigation system (INS), and operator controls via the mission processor, and performs as a master controller for the radar hardware.

Coherent processing requires that all frequency down-conversions, including the final conversion to baseband, retain the coherent phase relationship between transmitted and received pulses. All the local oscillators are phase referenced to the same *master oscillator*, which is also used to produce the transmitted waveform. The *in-phase* (I) and *quadrature* (Q) components at baseband represent the real and imaginary parts, respectively, of a complex number whose complex argument in phasor notation is the phase difference between the transmitted and received pulses. The complex modulus, or magnitude, is proportional to the received echo strength.

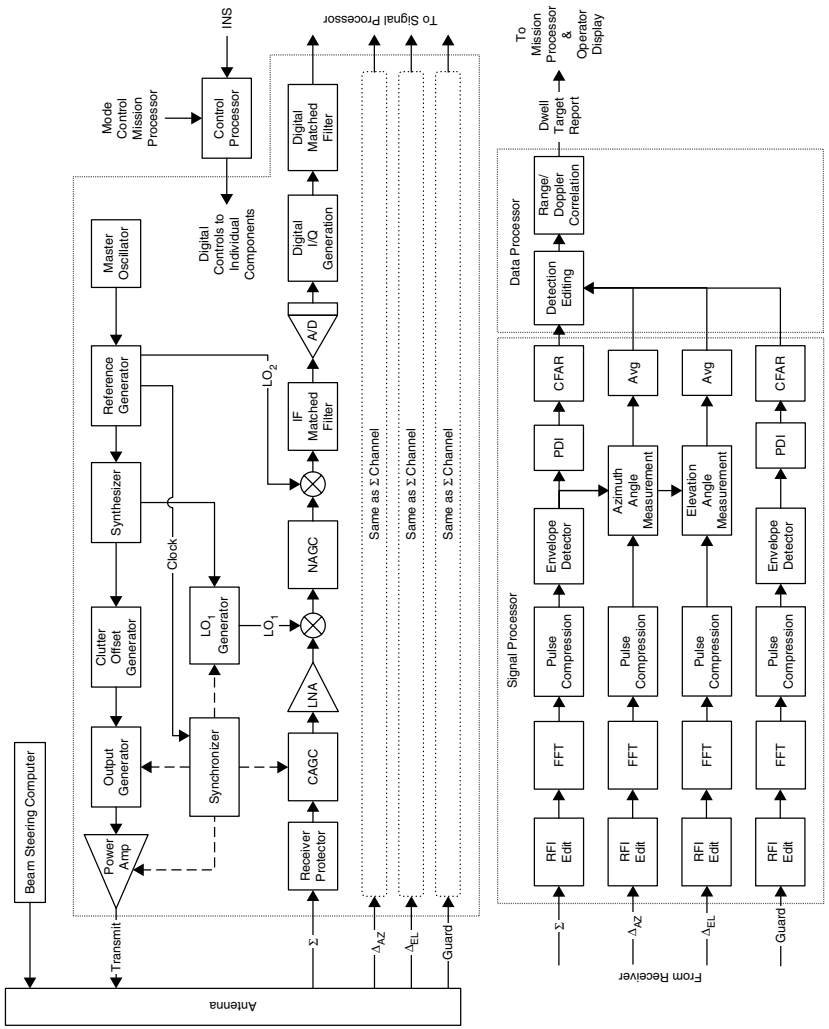

FIGURE 4.8 Typical pulse doppler radar configuration

Master Oscillator. The master oscillator provides a free-running, stable reference sinusoid on which the system synchronization is based.

Synchronizer. The synchronizer distributes precisely timed strobes and clocks for the various components of the radar system to ensure the time alignment of transmit waveforms and the reception of their corresponding returns. These low-jitter timing signals are used to enable and disable the transmit power amplifier to create the transmit pulse train, blank the receiver during transmission, and form the range gates.

Reference Generator. The reference generator outputs fixed frequency clocks and local oscillators (LOs).

Synthesizer. The synthesizer generates the transmit carrier frequency and the first local oscillator (LO_1) frequency. Frequency agility is provided to the transmit and LO_1 signals.

Clutter Offset Generator. The clutter offset generator shifts the transmit carrier slightly, so that on receive the main-beam clutter is positioned at zero doppler frequency, or DC (direct current) after basebanding. The same effect could be obtained by shifting the receiver LO_1 frequency. With the clutter at DC, the spurious signals caused by certain receiver nonlinearities, such as mixer intermodulation products and video harmonics, also fall near DC and can be filtered out along with the main-beam clutter.[19] The frequency shift applied is a function of the antenna main-beam line-of-sight relative to the platform's velocity vector. This process is known as *clutter positioning*.

Output Generator. The output generates the pulsed radio frequency (RF) transmit signal, which is the transmit drive signal that is amplified by the power amplifier prior to being fed to the transmit antenna.

Antenna. The antenna can be mechanically or electronically scanned. Modern pulse doppler radars have migrated to the use of active electronically scanned arrays (AESAs).[20] AESAs contain transmit/receive (T/R) modules, each comprising a transmit power amplifier and a receive low-noise amplifier (LNA) along with an attenuator and phase shifter, at each antenna element.

If the same antenna is used for transmit and receive, a duplexer must be included. This duplexer is usually a passive device, such as a circulator, which effectively switches the antenna between the transmitter and receiver. Considerable power may be coupled to the receiver since typically no more than 20 to 25 dB of isolation may be expected from ferrite circulators.

Antennas may form various beams. The transmit beam can be formed with uniform aperture illumination to maximize the amount of energy on target, whereas the receive sum (Σ) beam is typically formed with a low-sidelobe taper to minimize the returns from ground clutter. The Σ beam is used for target detection and, acting as a spatial filter, is the first line of defense against clutter and interference in the sidelobe region. To facilitate target tracking, angle measurements with accuracies finer than the antenna beamwidth are usually required. A technique to obtain such angle measurements of a target on a single pulse is called *monopulse*. Monopulse can be characterized as amplitude or phase, with phase being preferable due to its advantage in angle accuracy for a given signal-to-noise ratio. Phase monopulse uses a *delta* or difference beam,

which is essentially formed by dividing the aperture into two halves and subtracting the corresponding phase centers. Monopulse beams, delta-azimuth (Δ_{AZ}) and delta-elevation (Δ_{EL}), are formed to provide phase monopulse azimuth and elevation angle measurements.[21] Self-calibration routines controlled by the control processor ensure that the phase and amplitude match of the receiver channels enables accurate monopulse measurements. A guard beam with a near-omnidirectional pattern is formed for sidelobe detection blanking as discussed in Section 4.2.

Receiver/Protector (R/P). The receiver/protector is a low-loss, fast-response, high-power switch that prevents the transmitter output from the antenna's duplexer from damaging the sensitive receiver front end. Fast recovery is required to minimize desensitization in the range gates following the transmitted pulse. R/Ps can be implemented with a gas discharge tube, in which a gas is ionized by high-power RF. A diode limiter can be used instead of or in conjunction with the gas discharge tube. The R/P can be reflective or absorptive, but must have low insertion loss to minimize impact on receive chain noise figure.

Clutter Automatic Gain Control (CAGC). The CAGC attenuator is used both for suppressing transmitter leakage from the R/P into the receiver (so the receiver is not driven into saturation, which could lengthen recovery time after the transmitter is turned off) and for controlling the input signal levels into the receiver. The received levels are kept below saturation levels, typically with a clutter AGC in search and a target AGC in single-target track, to prevent spurious signals, which degrade performance, from being generated.

Noise Automatic Gain Control (NAGC). The NAGC attenuator is used to set the thermal noise level in the receiver to support the required dynamic range, as discussed in Section 4.3. The attenuation is commanded based on measurements of the noise during periodic calibration.

Digital Preprocessing. The advent of high-speed, high-dynamic range analog-to-digital converters (A/Ds) allows IF-sampling and digital basebanding. The digital IF-sampled output of the receiver is downconverted to baseband (DC) via a digital product detector (DPD).[22] Superior I/Q image rejection is an advantage of a DPD.

The I and Q signals are passed through the digital portion of the pulse matched filter. The combination of the IF matched filter and the digital matched filter form the receiver's single-pulse matched filter.

Digital Signal Processing. Following digital preprocessing is a doppler filter bank for main-beam clutter rejection and coherent integration. RF interference (RFI) that is pulsed and asynchronous to the radar timing can often be detected prior to the coherent integration. Range-IPP cells where RFI is detected are then "repaired" to prevent corruption of the output spectrum. The filter bank is usually realized by using the fast Fourier transform (FFT); however, the discrete Fourier transform (DFT) can be used when the number of filters is small. Appropriate weighting is employed to reduce the filter sidelobes. The amount of weighting can be chosen adaptively by sensing the peak signal levels (usually main-beam clutter) and selecting the doppler weighting dynamically.

If pulse compression modulation is used on the transmit pulse to increase energy on target, pulse compression can be performed digitally either before or after the doppler

filter bank. The advantage of pulse compression after the filter bank is that the effects of doppler on pulse compression can be largely removed by tailoring the pulse compression to the doppler offset of each doppler filter. However, this increases the total amount of signal processing required.

The envelope at the output of the FFT is formed with a linear ($\sqrt{I^2+Q^2}$) or square-law (I^2+Q^2) detector. Historically, linear detectors were used to manage dynamic range in fixed-point processors. Square-law detectors are preferred for some modern floating-point processors. Postdetection integration (PDI) may be used where each range-gate–doppler-filter output is linearly summed over several CPIs. For each range-doppler cell in the Σ channel, the PDI output is compared with a detection threshold determined by a constant-false-alarm-rate (CFAR) process.[23–26] Cells with amplitudes greater than the CFAR threshold are labeled as detections.

Similar processing is done in the Δ_{AZ} and Δ_{EL} channels with exceptions, as shown in Figure 4.8. For those range-doppler cells with declared detections, the imaginary part of the Δ_{AZ}/Σ and Δ_{EL}/Σ ratios are used for phase comparison monopulse to estimate the azimuth and elevation angles, respectively, relative to the center of the Σ main beam. The angle estimates are computed for each coherent look and then averaged over the number of CPIs noncoherently integrated via PDI.

The guard channel is processed similar to the Σ channel. The guard channel's purpose is to blank sidelobe detections, as described in Section 4.2.

Postprocessing. Following the CFAR is detection editing, which contains the sidelobe discrete rejection logic. Following detection editing, range and velocity ambiguity resolvers work over several looks within a dwell. The final detection outputs, along with their corresponding unambiguous range, velocity, and angle measurements, and their estimated accuracies, are passed to the mission processor for tracking and operator display.

4.2 PULSE DOPPLER CLUTTER

General. Clutter returns from various scatterers have a strong influence on the design of a pulse doppler radar as well as an effect on the probability of detection of point targets. Clutter scatterers include terrain (both land and sea), weather (rain, snow, etc.), and chaff. Since the antennas generally used in pulse doppler radars have a single, relatively high-gain main beam, main-beam clutter may be the largest signal handled by the radar when in a down-look condition. The narrow beam limits the frequency extent of this clutter to a relatively small portion of the doppler spectrum. The remainder of the antenna pattern consists of sidelobes, which result in sidelobe clutter. This clutter is generally much smaller than the main-beam clutter but covers much more of the frequency domain. The sidelobe clutter from the ground directly below the radar, the altitude-line, is frequently large owing to a high reflection coefficient at steep grazing angles, the large geometric area, and the short range. Range performance is degraded for targets in the sidelobe clutter region wherever the clutter is near or above the receiver noise level. Multiple PRFs may be used to move the target with respect to the sidelobe clutter in the range-doppler map, thus avoiding completely blind ranges or blind frequencies due to high clutter levels. This relative motion occurs due to the range and doppler foldover from range and/or doppler ambiguities. If one PRF folds sidelobe clutter and a target to the same apparent range and doppler, a sufficient change of PRF will separate them.

Ground Clutter in a Stationary Radar. When the radar is fixed with respect to the ground, both stationary main-beam and sidelobe clutter returns occur at zero-doppler offset from the transmit carrier frequency. The sidelobe clutter is usually small compared with main-beam clutter as long as some part of the main beam strikes the ground. The clutter can be calculated as in a pulsed radar, then folded in range as a function of the PRF.

Ground Clutter in a Moving Radar. When the radar is moving with a velocity V_R, the clutter is spread over the frequency domain as illustrated in Figure 4.2 for the special case of horizontal motion. The foldover in range and doppler is illustrated in Figure 4.9 for a medium-PRF radar where the clutter is ambiguous in both range and doppler. The radar platform is moving to the right at 1000 kt with a dive angle of 10°. The narrow annuli (iso-range contours) define the ground area that contributes to clutter in the selected range gate. The five narrow hyperbolic bands (iso-doppler contours) define the area that contributes to clutter in the selected doppler filter. The shaded intersections represent the area, or clutter patches, that contributes to the range-gate–doppler-filter cell. Each clutter patch contributes clutter power as a function of the antenna gain in the direction of the clutter patch and the reflectivity of the clutter patch.

The main beam illuminates the elliptical area to the left of the ground track. Since this area lies entirely within the filter area, the main-beam clutter falls within this filter, and all other filters receive sidelobe clutter. Four range annuli are intersected by the main-beam ellipse, so the main-beam clutter in this range gate is the vector sum of the signals received from all four clutter patches. Owing to this high degree of range foldover, all range gates will have approximately equal clutter.

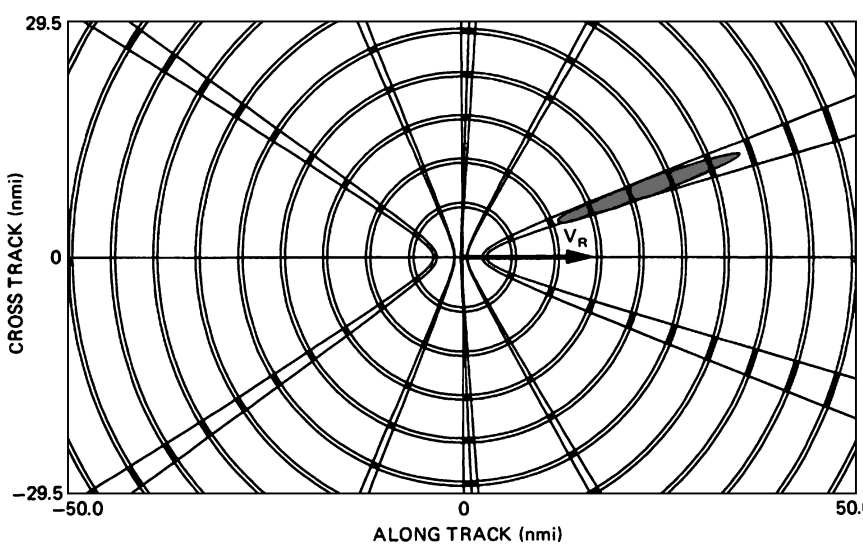

FIGURE 4.9 Plan view of range-gate and doppler-filter areas. Radar altitude = 10,000 ft; velocity = 1000 kt to right; dive angle = 10°; radar wavelength = 3 cm; PRF = 15 kHz; range gate width = 6.67 μs; range gate = 4; doppler filter at 2 kHz; bandwidth = 1 kHz; beamwidth = 5° (circular); main-beam azimuth = 20°; depression angle = 5°.

If the main beam were scanned 360° in azimuth with the same radar platform kinematics, the main-beam clutter would scan in doppler frequency so that it would appear in the selected filter ten times (twice for each hyperbolic band). In between, the filter would receive sidelobe clutter from all darkened intersections. With the use of the proper clutter offset (which would vary as a function of main-beam azimuth) on the transmit frequency, as described in Section 4.1, the doppler of the main-beam clutter return will be zero or DC.

Clutter Return: General Equations. The clutter-to-noise ratio from a single clutter patch with incremental area dA at a range R is

$$C/N = \frac{P_{av} G_T G_R \lambda^2 \sigma^0 dA}{(4\pi)^3 R^4 L_C k T_s B_n} \tag{4.2}$$

where P_{av} = average transmit power
G_T = transmit gain in patch direction
G_R = receive gain in patch direction
λ = operating wavelength
σ^0 = clutter backscatter coefficient
L_C = losses applicable to clutter
k = Boltzmann's constant = 1.38054×10^{-23} W/(Hz/K)
T_s = system noise temperature, K
B_n = doppler filter bandwidth

L_C refers to losses that apply to distributed surface clutter, as opposed to discrete, resolvable targets. These losses will be discussed in Section 4.6.

The clutter-to-noise ratio from each radar resolution cell is the integral of Eq. 4.2 over the doppler and range extent of each of the ambiguous cell positions on the ground.[27–31] Under certain simplified conditions, the integration can be closed-form,[32] but in general, numeric integration is required.

Main-beam Clutter. The net main-beam clutter-to-noise power in a single range gate in the receiver can be approximated from Eq. 4.2 by substituting the range gate's intersected area ($\frac{c\tau}{2\cos(\alpha)} R\theta_{az}$) within the main beam on the ground for dA and summing over all ambiguities of that range gate that are within the main beam.[33]

$$\frac{C}{N} = \frac{P_{av} \lambda^2 \theta_{az} (c\tau/2)}{(4\pi)^3 L_C k T_s B_n} \sum \frac{G_T G_R \sigma^0}{R^3 \cos(\alpha)} \tag{4.3}$$

The summation limits are the lower and upper edges in the elevation dimension of the smaller of the transmit and receive beams

where θ_{az} = azimuth half-power beamwidth, radians
τ = compressed pulse width
α = grazing angle at clutter patch

The remaining terms are as defined following Eq. 4.2.

If the main beam is pointed below the horizon, the main-beam clutter spectral width Δf due to platform motion measured 6 dB down from the peak is approximately[34]

$$\Delta f = \frac{2V_R}{\lambda} \left\{ \theta_B \cos(\phi_0) \sin(\theta_0) + \frac{\theta_B^2 \cos(\phi_0)\cos(\theta_0)}{8} + \frac{c\tau \sin^3(\phi_0)\cos(\theta_0)}{2h\cos(\phi_0)} \right\} \tag{4.4}$$

where V_R = radar ground speed
λ = RF wavelength
θ_B = 3 dB one-way antenna azimuth beamwidth, radians
ϕ_0 = main-beam depression angle relative to local horizontal, radians
θ_0 = main-beam azimuth angle relative to the horizontal velocity, radians
τ = compressed pulse width
h = radar altitude

When the magnitude of the main-beam azimuth angle is greater than half of the azimuth beamwidth ($|\theta_0| \geq \theta_B/2$), the main-beam clutter power spectral density can be modeled with a gaussian shape with a standard deviation $\sigma_c = 0.3\Delta f$.

Main-beam Clutter Filtering. In a pulse doppler radar utilizing digital signal processing, main-beam clutter is rejected by either a combination of a delay-line clutter canceler (MTI filter) followed by a doppler filter bank or by a filter bank with low filter sidelobes, which are achieved via weighting.[35] In either case, the filters around the main-beam clutter are blanked to minimize false alarms on main-beam clutter. This blanked region in doppler is known as the main-beam clutter *notch*.

The choice between these options is a trade-off of quantization noise and complexity versus the filter-weighting loss. If a canceler is used, filter weighting can be relaxed over that with a filter bank alone, since the canceler reduces the dynamic-range requirements into the doppler filter bank (if the main-beam clutter is the largest signal). Without a canceler, heavier weighting is needed to reduce sidelobes to a level so that the filter response to main-beam clutter is below the thermal-noise level. This weighting increases the filter noise bandwidth and hence increases the loss in signal-to-noise ratio.

Choosing the proper weighting is a compromise between rejecting main-beam clutter and maximizing target signal-to-noise ratio. To dynamically make this compromise, the filter weighting can be adaptive to the main-beam clutter level by measuring the peak return level (usually main-beam clutter) over the IPPs, and selecting or computing the best weighting to apply across the CPI. Another technique that is applicable to high-medium and high PRF is to generate a hybrid filter weighting by convolving two weighting functions. The result is a filter with significantly less weighting loss and low far-out sidelobes, but at a cost of relatively high near-in sidelobes.

To evaluate the effect of main-beam clutter on target detection performance, the clutter-to-noise ratio must be known for each filter where targets are to be detected. A general measure that can be easily applied to specific clutter levels is the improvement factor I. When using a doppler filter bank, as opposed to an MTI filter, the improvement factor is defined for each doppler filter as the ratio of the signal-to-clutter power at the output of the doppler filter to the signal-to-clutter power at the input.[36] The signal is assumed to be at the center of the doppler filter. Incorporating the effect of filter weighting, the improvement factor for a doppler filter is given by[37]

$$I(K) = \frac{\left[\sum_{n=0}^{N-1} A_n\right]^2}{\sum_{n=0}^{N-1}\sum_{m=0}^{N-1} A_n A_m \exp\left\{-2\left[\pi(n-m)\sigma_c T\right]^2\right\}\cos\left[2\pi K(n-m)/N\right]} \tag{4.5}$$

where A_i = IPP weight, $0 \le i \le N-1$
N = number of IPPs in CPI
σ_c = standard deviation of clutter spectrum
K = filter number ($K = 0$ is the DC filter)
T = interpulse period

Clutter-transient Suppression. When (1) the PRF is changed for multiple-PRF ranging, (2) the slope is changed in linear FM ranging, or (3) the RF carrier is changed, the transient change in the clutter return may cause degradation unless it is properly handled.[38] Since the clutter is usually ambiguous in range in a pulse doppler radar, the clutter power increases at each interpulse period (IPP) as clutter return is received from the farther ambiguities, until the horizon is reached. This phenomenon is called *space charging*. Note that although an increasing number of clutter returns are received during the charging period, the vector sum may actually decrease owing to the random phase relations of the returns from different patches.

If a clutter canceler (MTI filter) is used, the output cannot begin to settle to its steady-state value until space charging is complete. Some settling time must be allowed before signals are passed to the filter bank. Therefore, the coherent integration time available during each CPI is reduced from the total CPI time by the sum of the space charge time and the transient settling time. The canceler settling time can be eliminated by *precharging* the canceler with the steady-state input value.[39] This is done by changing the canceler gains so that all delay lines achieve their steady-state values on the first IPP of data.

If no canceler is used, signals can be passed to the filter bank after the space charge is complete, so that the coherent integration time is the total CPI time minus the space charge time.

Altitude-line Clutter Blanking. The reflection from the earth directly beneath an airborne pulse radar is called altitude-line clutter. Because of specular reflection over smooth terrain, the large geometric area, and relatively short range, this signal can be large. It lies within the sidelobe clutter region of the pulse doppler spectrum.

Because it can be much larger than diffuse sidelobe clutter and usually has a relatively narrow spectral width, altitude-line clutter is often removed either by a special CFAR that prevents detection of the altitude-line, or by a tracker-blanker that removes these reports from the final output. In the case of the tracker-blanker, a closed-loop tracker is used to position range and velocity gates around the altitude return and blank the affected range-doppler region. Note that at very low altitudes, the angles that subtend the first range gate on the ground can be quite big, and the spectral width widens.

Sidelobe Clutter. The entire clutter spectrum can be calculated for each range gate by Eq. 4.2 if the antenna pattern is known in the lower hemisphere. In preliminary system design, the exact gain function may not be known, so one useful approximation is that the sidelobe radiation is isotropic with a constant gain of G_{SL}.

Sidelobe Discretes. An inherent characteristic of airborne pulse doppler radars is that echoes from large, resolvable objects on the ground (discretes), such as buildings, may be received through the antenna sidelobes and appear as though they were

smaller moving targets in the main beam. This is a particularly severe problem in a medium-PRF radar, where all-aspect target performance is usually desired, since these returns compete with targets of interest. In a high-PRF radar, there is little if any range region clear of sidelobe clutter, such that the sidelobe clutter portion of the doppler spectrum is often not processed (since target detectability is severely degraded in this region). Further, in a high-PRF radar, especially at higher altitudes, the relative amplitudes of the distributed sidelobe clutter and the discrete returns are such that the discretes are not visible in the sidelobe clutter.

The apparent radar cross section (RCS), σ_{app}, of a sidelobe discrete with an RCS of σ is $\sigma_{app} = \sigma G_{SL}^2$, where G_{SL} is the sidelobe gain relative to the main beam. The larger-size discretes appear with a lower density than the smaller ones, and a model commonly assumed at the higher radar frequencies is shown in Table 4.4. Thus, as a practical matter, 10^6 m^2 discretes are rarely present, 10^5 m^2 are sometimes present, and 10^4 m^2 are often present.

Two mechanizations for detecting and eliminating false reports from sidelobe discretes are the guard channel and postdetection sensitivity time control (STC). These are discussed in the paragraphs that follow.

Guard Channel. The guard channel mechanization compares the outputs of two parallel receiving channels, one connected to the main antenna and the second to a guard antenna (the Σ and Guard channel in Figure 4.8, respectively), to determine whether a received signal is in the main beam or the sidelobes.[40–44] The guard channel uses a broad-beam antenna that (ideally) has a pattern above the main-antenna sidelobes. The returns from both channels are compared for each range-doppler cell that had a detection in the main channel. For these range-doppler cells, when the guard channel return is greater than that of the main channel, the detection is rejected (blanked). If the main channel return is higher, the detection is passed on.

A block diagram of a guard channel mechanization is shown in Figure 4.10. After the CFAR (which ideally would be identical in both channels), there are three thresholds: the main channel, guard channel, and main-to-guard-ratio thresholds. The detection logic of these thresholds is also shown in Figure 4.10.

The blanking that occurs because of the main/guard comparison affects the detectability in the main channel, the extent of which is a function of the threshold settings. The threshold settings are a tradeoff between false alarms due to sidelobe returns and detectability loss in the main channel. An example is shown in Figure 4.11 for a nonfluctuating target, where the ordinate is the probability of detection in the final output of the sidelobe blanker and the abscissa is the signal-to-noise ratio (SNR) in the main channel. The quantity B^2 is the ratio of the guard channel SNR to the main channel SNR and is illustrated in Figure 4.12.

TABLE 4.4 Discrete Clutter Model

Radar Cross Section (m^2)	Density (per square mile)
10^6	0.01
10^5	0.1
10^4	1

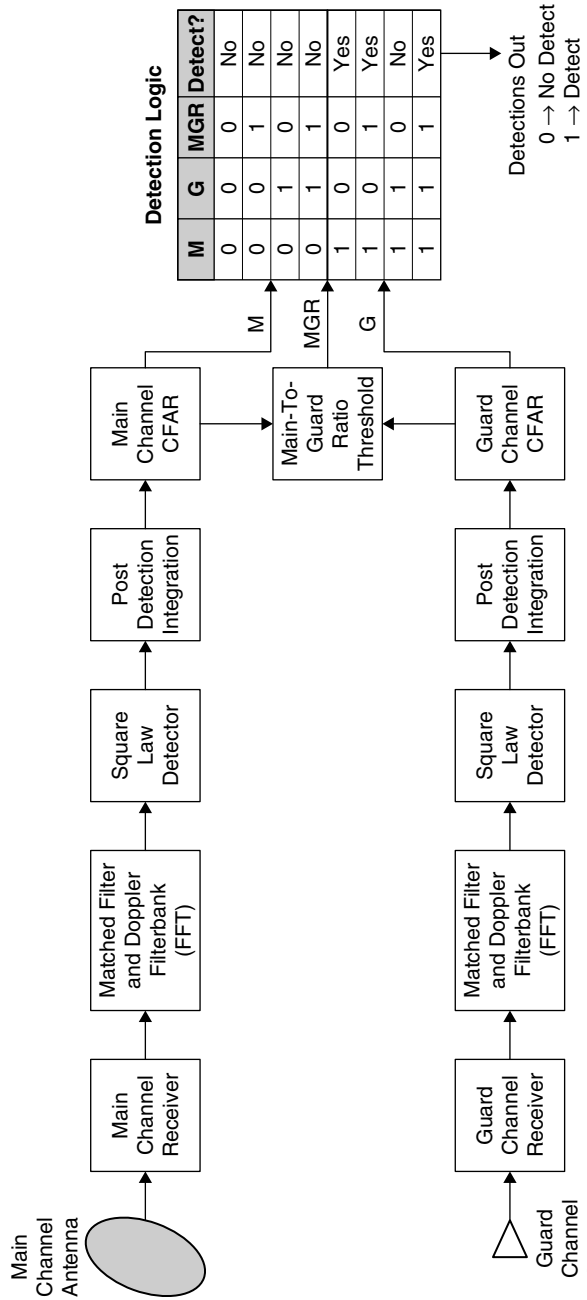

FIGURE 4.10 Two-channel sidelobe blanker

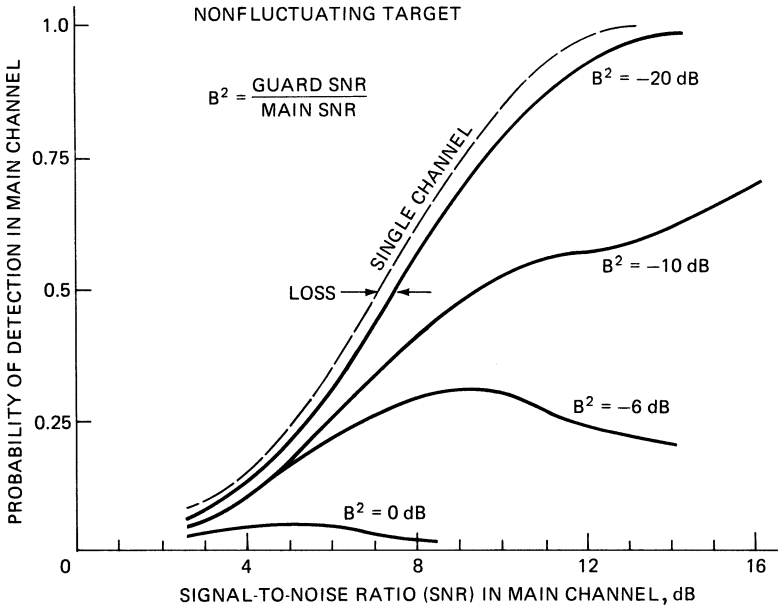

FIGURE 4.11 Probability of detection versus signal-to-noise ratio with a guard channel

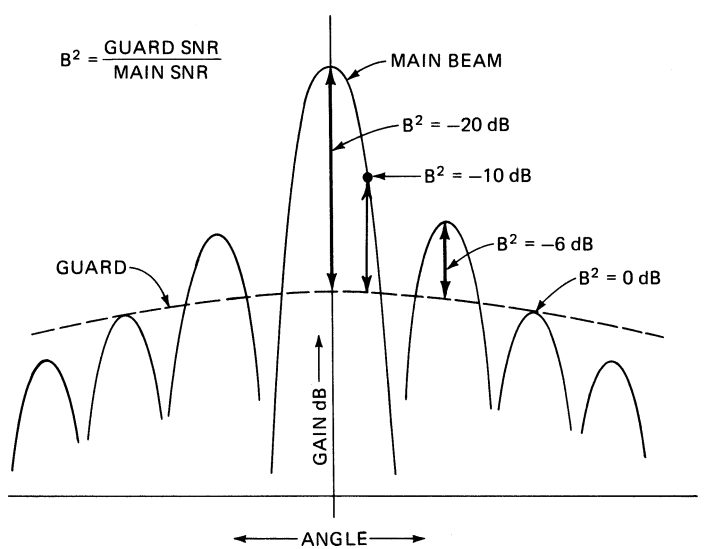

FIGURE 4.12 Main and guard antenna patterns

B^2 is small for a target in the main beam and large, 0 dB or so, for a target at the sidelobe peaks. In the example shown, there is a 0.5 dB detectability loss due to the guard blanking for targets in the main beam.

Ideally, the guard antenna gain pattern exceeds that of the main antenna at all angles in space (except for the main beam) to minimize detections through the sidelobes. If not, however, as illustrated in Figure 4.11 and Figure 4.12, returns through the sidelobe peaks of the main pattern above the guard pattern have a significant probability of detection in the main channel and would represent false detections.

Postdetection STC. In the ambiguity resolution, as the output returns are range-correlated, they are subjected to postdetection STC, or RCS thresholding, applied inside the range correlation process. Target returns that range correlate inside the STC range, but fall below the STC threshold, are likely sidelobe discretes and are blanked or removed from the correlation process (and kept from ghosting with other targets).

The basic logic is shown in Figure 4.13.[45] Basically, the CFAR output data is correlated (resolved) in range three times. Each correlator calculates unambiguous range using M out of the N sets of detection data (e.g., three detections required out of eight PRFs). No doppler correlation is used since the doppler is ambiguous. The results of the first two correlations are used to blank all outputs that are likely to be sidelobe discretes from the final range correlator. Here, three range correlators are used in which the first, the A correlator, resolves the range ambiguities within some nominal range, say, 10 nm, beyond which sidelobe discretes are not likely to be detected. A second correlator, the B correlator, resolves the range ambiguities out to the same range, but before a target can enter the B correlator, its amplitude is thresholded by a range-varying threshold (the STC threshold). A range gate by range gate comparison is made of the correlations in the A and B correlators, and if a range gate correlates in A and not in B, that gate is blanked out of the third correlator, the C correlator. The C correlator resolves the range ambiguities within the maximum range of interest. An alternative mechanization is to replace the range-varying STC with an equivalent RCS threshold inside the range correlation process. The RCS is computed for each possible unfolded range (starting from the shortest range) and compared to the RCS threshold. Detections that range correlate, but are below the RCS threshold, are prevented from correlating with other detects (and all of their unfolded ranges are also prevented from correlating).

The principle behind the postdetection STC approach is illustrated in Figure 4.14, where the return of a target in the main beam and a large discrete target in the sidelobes is plotted versus unambiguous range (that is, after the range ambiguities have been resolved). Also shown are the normal CFAR threshold and the STC threshold versus range. A discrete return in the sidelobes is below the STC threshold, and a return in the main beam is above the threshold, such that the sidelobe discrete can be recognized and blanked without blanking the target in the main beam. The STC onset range represents the range at which a large discrete target in the sidelobes exceeds the CFAR threshold.

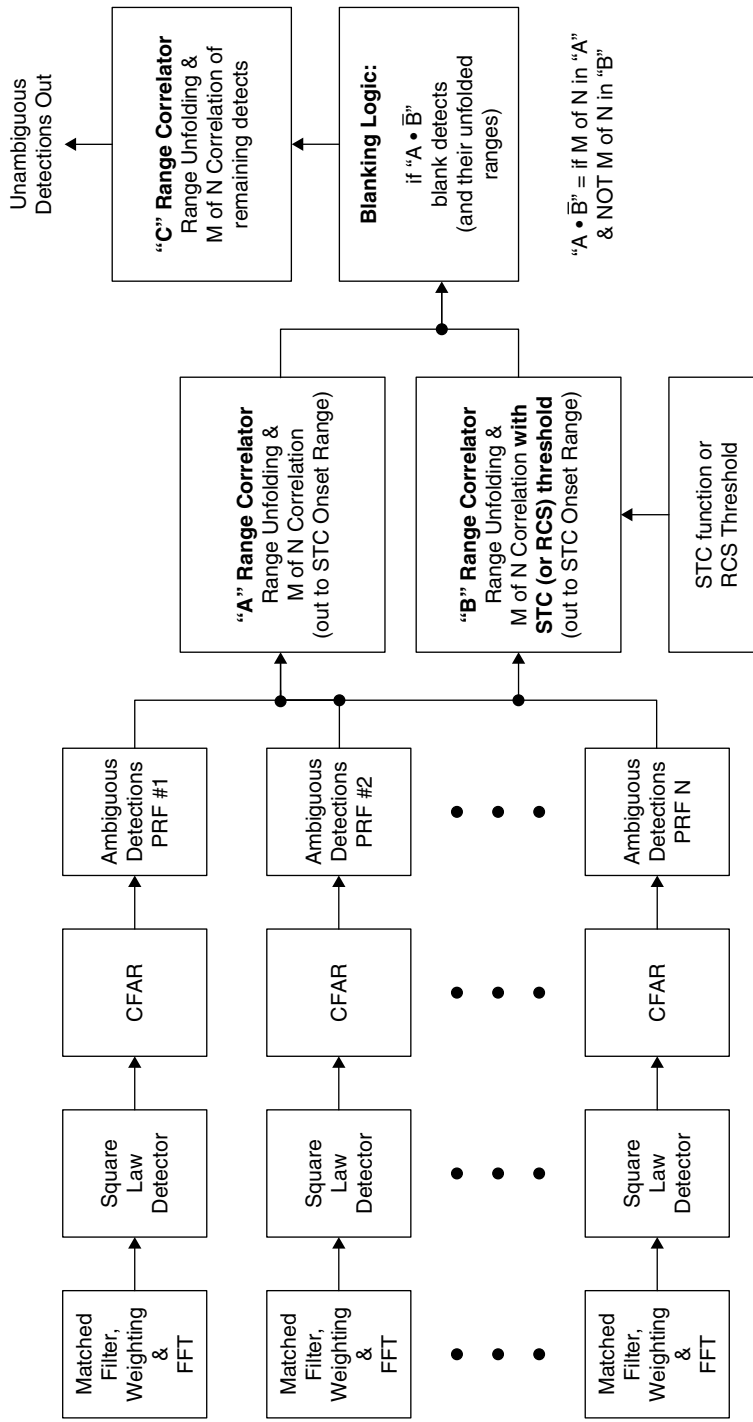

FIGURE 4.13 Single-channel sidelobe blanker using postdetection STC or RCS thresholding to remove sidelobe discretes.

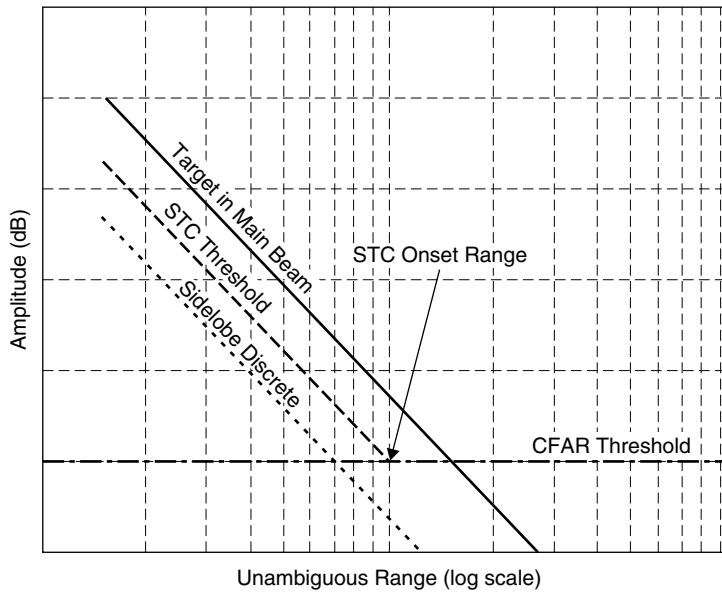

FIGURE 4.14 Postdetection STC levels

4.3 DYNAMIC-RANGE AND STABILITY REQUIREMENTS

Doppler processing separates moving targets from clutter and allows them to be detected while only competing against thermal noise, assuming that the targets have sufficient radial velocity ($> 2V_R/\lambda$) and the PRF is high enough for an unambiguous clutter spectrum. Coherence, the consistency of phase of a signal's carrier frequency from one pulse to the next, is crucial for doppler processing. Without careful system design, amplitude and phase instabilities during the coherent integration time will broaden the main-beam clutter spectrum and raise the noise floor that clutter-free targets must compete with for detection. Nonlinearities in the system can also cause discrete spurious spectral signals that can be mistaken as targets. The instantaneous dynamic range of the system governs the system linearity and hence sensitivity in a strong clutter environment. The driving factor upon stability requirements is when the main-beam clutter level is at the saturation point of the receiver.

Dynamic Range. Dynamic range, as discussed here, can be referred to as *instantaneous dynamic range* and is the linear region above thermal noise over which the receiver and signal processor operate before any saturation (clipping) or gain limiting occurs. If saturations occur, spurious signals that degrade performance may be generated. For example, if main-beam clutter saturates, spurious frequencies can appear in the doppler passband normally clear of main-beam clutter, and this may generate false-target reports. An automatic gain control (AGC) function is often employed to prevent saturations on either main-beam clutter in search or the target in Single-Target Track mode. However, the use of AGC degrades the system's sensitivity, so large

instantaneous dynamic range is preferable. If saturations occur in a range gate during an integration period, an option in a multiple-range gated system is simply to blank detection reports from that gate. When a MTI filter is not used, the doppler filter bank for each range gate can be examined to determine if there are any detections due to spurious signals from large clutter, with subsequent editing of these detections if the measured clutter-to-noise ratio exceeds the dynamic range. Similar logic can be applied to saturated range gates to determine if the largest signal in the filter bank is in the passband or represents saturated clutter returns. Saturated returns with the peak signal in the doppler passband can represent valid targets at short ranges and need not be subjected to the sidelobe blanking logic.

The most stressing dynamic-range requirement is due to main-beam clutter when searching for a small, low-flying targets. Here, full sensitivity must be maintained in the presence of the clutter to maximize the probability of detecting the target.

The dynamic-range requirement of a pulse doppler radar, as determined by main-beam clutter, is a function not only of the basic radar parameters such as power, antenna gain, etc., but of radar altitude above the terrain and the radar cross section (RCS) of low-flying targets. As an example, Figure 4.15 shows the maximum clutter-to-noise ratio (C/N_{max}) that appears in the ambiguous-range interval, i.e., after range folding, for a medium-PRF radar as a function of radar altitude and the range of the intersection of the peak of the main-beam with the ground. Note that the clutter-to-noise ratio is a rms power ratio measured at the A/D converter. A peak power ratio would be 3 dB higher.

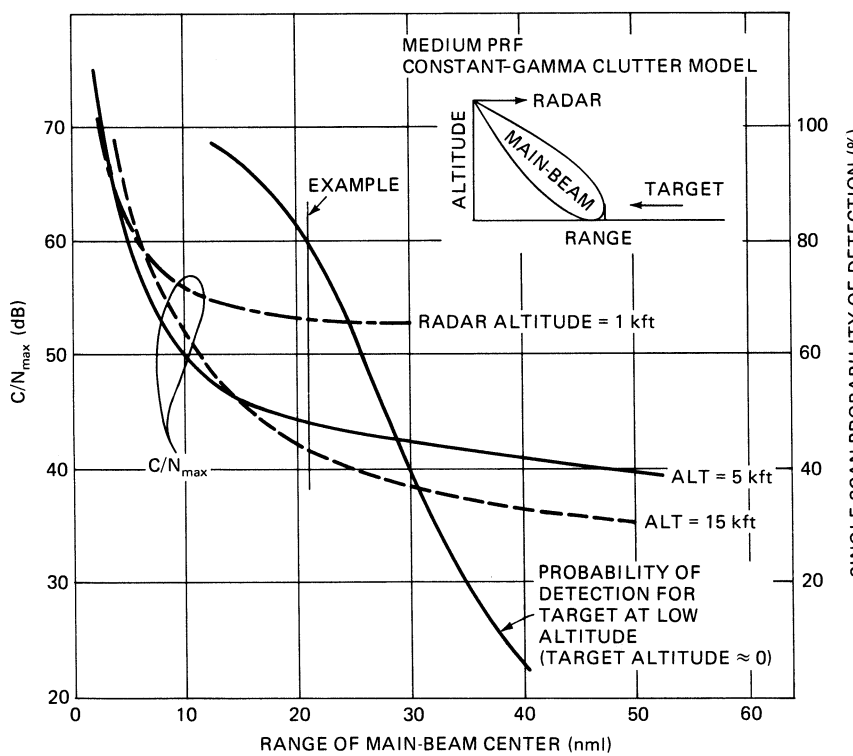

FIGURE 4.15 Dynamic-range example

The amplitude of clutter returns fluctuate over time and are modeled as a stochastic process. The clutter-to-noise ratio represents the mean value of this process over time. Figure 4.15 assumes a pencil-beam antenna pattern and a constant-gamma model for clutter reflectivity.[46] The antenna beam is pointed at the ground corresponding to the range of the target. At longer ranges (small look-down angles), clutter decreases with increasing radar altitude since range folding is less severe owing to less of the main beam intersecting the ground. At shorter ranges, clutter increases with radar altitude since the clutter patch size on the ground increases. While Figure 4.15 is for a medium-PRF radar, similar curves result for a high-PRF radar.

Also shown in Figure 4.15 is the single-scan probability of detection P_d versus range for a given RCS target in a receiver with unlimited dynamic range. If it is desired to have the low-flying target reach at least, say, an 80% P_d before any gain limiting (i.e., the use of AGC) occurs, the dynamic-range requirement is driven by the main-beam clutter levels $C/N_{\max}$ of 53 dB at 1000 ft, 44 dB at 5000 ft, and 41 dB at 15,000 ft for this example. The higher the desired probability of detection or the lower the radar altitude, the more dynamic range is required. Further, if the specified target RCS is reduced, the dynamic-range requirement for the same desired P_d increases as the P_d-versus-range curve in Figure 4.15 shifts to the left.

In a pulse doppler radar using digital signal processing, the A/D converters are usually selected to have a dynamic range that meets or exceeds the usable dynamic range set by the maximum clutter-to-noise ratio ($C/N_{\max}$) and the system stability. The peak dynamic range, defined as the maximum peak sinusoidal signal level relative to the rms thermal-noise level that can be processed linearly, is related to the number of amplitude bits in the A/D converter by

$$\left[\frac{S_{\max}}{N}\right]_{\text{dB}} = 20\log_{10}\left(\frac{2^{N_{\text{AD,amp}}}-1}{[\text{noise}]_{\text{quanta}}}\right) \tag{4.6}$$

where $[S_{\max}/N]_{\text{dB}}$ = maximum input peak sinusoidal level relative to rms noise, dB
$N_{\text{AD,amp}}$ = number of amplitude bits (not including sign bit) in the A/D converter
$[\text{noise}]_{\text{quanta}}$ = rms thermal-noise voltage level at the A/D converter, quanta

The rms thermal-noise voltage level at the A/D converter is given in terms of *quanta*. A single quanta refers to a unit quantization level of the A/D converter.

From the relationship described above and assuming the A/D converter limits the dynamic range, the A/D converter size can now be determined. Additional margin to allow for main-beam clutter fluctuations above the mean value also needs to be considered. Since main-beam clutter time fluctuation statistics are highly dependent on the type of clutter being observed, such as sea clutter or clutter from an urban area, and are generally unknown, a value of 10 to 12 dB above the rms value is often assumed for the maximum peak level (this also includes the 3 dB difference between the rms and peak values of a sinusoidal signal). Thus, the required number of amplitude bits in the A/D converter as determined by the main-beam clutter is

$$N_{\text{AD,amp}} \geq \text{CEIL}\left[\frac{[(C/N)_{\max}]_{\text{dB}} + [\text{fluct\_margin}]_{\text{dB}} + 20\log_{10}[[\text{noise}]_{\text{quanta}}]}{6}\right] \tag{4.7}$$

where CEIL(x) is the smallest integer $\geq x$. The instantaneous dynamic range supported by an A/D converter improves about 6 dB per bit.[47]

For the example cited in Figure 4.15, where the maximum C/N is 53 dB at a 1000-ft radar altitude and with a fluctuation margin of 10 dB and thermal noise at 1.414 quanta (3 dB), the A/D converter requires at least 11 amplitude bits plus a sign bit for a total of 12 bits to achieve the peak A/D dynamic range of 63 dB. The upper portion of Figure 4.16 illustrates this case. The lower portion of Figure 4.16 will be used in the stability discussion to follow.

Stability. To achieve the theoretical clutter rejection and target detection and tracking performance of a pulse doppler system, the reference frequencies, timing signals, and signal processing circuitry must be extremely stable.[48–52] In most cases, the major concern is with short-term rather than long-term stability. Long-term stability mainly affects velocity or range accuracy or spurious signals (due to PRF harmonics) but is relatively easy to make adequate. Short-term stability refers to variations within the round-trip radar echo time or during the signal coherent integration time. The most severe stability requirements relate to the generation of spurious modulation sidebands on the main-beam clutter, which raise the system noise floor or can appear as targets at the detectors. Thus, the maximum ratio of main-beam clutter to system noise measured at the receiver output (C/N), including the fluctuation margin as discussed above, is the predominant parameter that determines stability requirements.

Target returns compete with clutter returns and noise for detection. Suppose desired targets have sufficient radial speed so that they lie in the clutter-free region of doppler frequency when a pulse doppler waveform is used. These targets now have to compete only with system noise. This noise can be both additive and multiplicative. Additive noise tends to mask multiplicative noise in low-performance radars.

Additive noise sources can be external to the radar, such as atmospheric noise (sky temperature), ground noise (black body radiation), and jammers, or they can be internal, such as thermal noise. Thermal noise is also known as *Johnson noise* and

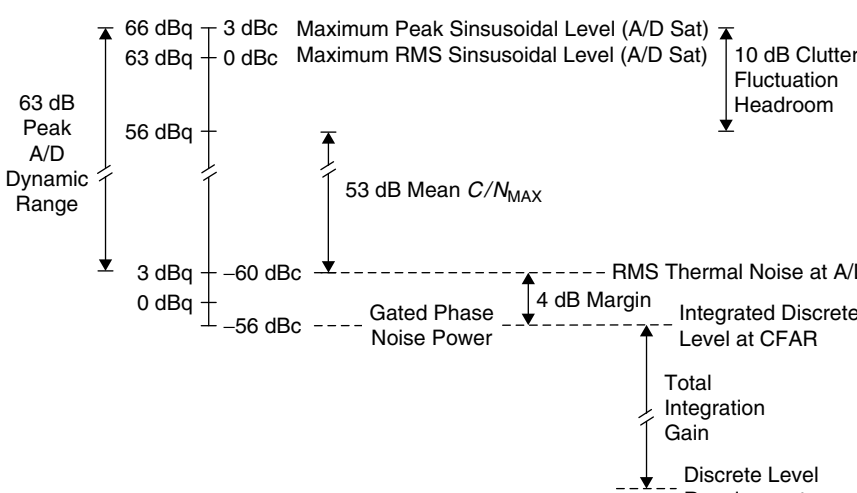

FIGURE 4.16 Dynamic range and stability levels

gaussian noise, the latter term arising from the gaussian statistics of its voltage probability density function. Thermal noise is always present in the radar receiver and is the ultimate limit on radar sensitivity. The absolute level of additive noise sources is determined by the source and its relation to the radar. Proper system design can reduce thermal noise to a level where multiplicative noise can become significant in limiting the radar sensitivity.

Multiplicative noise is characterized by either a time-varying amplitude (amplitude modulation, AM) or a time-varying phase (phase modulation, PM, or frequency modulation, FM). The absolute level depends on the strength of the signal (carrier) on which the noise source is riding. Multiplicative noise sources are frequency instabilities, power supply ripple and noise, 1/*f* noise, timing jitter, and unwanted mixer products (*discretes* or *spurs*). Multiplicative noise modulates radar returns by varying their amplitude or phase and is present on all radar returns being most apparent on large returns such as main-beam clutter. The result in the spectral domain is spurious modulation sidebands. Random multiplicative noise broadens the spectrum of the carrier frequency. Discrete multiplicative noise sources generate discrete spectral lines that can cause false alarms.

System stability is characterized by the overall two-way (transmit and receive) composite system frequency response, which is the return of a nonfluctuating target as a function of doppler frequency. System frequency response should be defined by the doppler passband.[53] The focus of this section will be the stability requirements for doppler frequencies separated enough from the carrier to be outside the ground moving target notch. The concern in this region is white phase noise, which determines the phase noise floor. Low frequency (i.e., closer to the carrier) stability is more applicable to air-to-ground pulse doppler modes such as GMTI and SAR.

The location of an instability source within the system will determine whether it is imparted upon a return signal via the transmit path, receive path, or both. Instabilities either on transmit or receive are called *independent*. Those imposed on both transmit and receive are *common*.

Amplitude instabilities caused by AM tend to be considered independent since the LOs drive the mixers in the receiver into compression. Also, transmitters work most efficiently when driven into compression (i.e., where the power amplifier is saturated and provides a constant output power level regardless of small deviations on the input). Instabilities due to PM (of which FM is a special case) tend to dominate those due to AM. As such, the focus will be on phase disturbances: random phase noise and discrete sinusoidal signals (spurious signals).

Random Phase Noise. Random phase noise riding on a large signal can mask weak target returns. The object is to specify system phase noise so that it is well below the thermal noise when a large signal at the A/D saturation level is present in the receiver. (A signal at A/D saturation is the largest signal that can be linearly processed by the radar receiver.) Then the radar sensitivity is limited by thermal noise (always present) plus a small increase in the total noise level caused by the phase noise.

The phase noise of oscillators and other components is typically specified as the multiplicative noise that rides on a continuous waveform, or CW phase noise. In pulse doppler radar, transmit gating interrupts the continuous waveform to produce a pulsed waveform. *Gated* phase noise is the result of gating CW phase noise. The spectrum of a pulsed (gated) signal is different from CW. The resulting noise, the gated noise, can be much different from the CW noise, especially for low duty cycle waveforms and noise close to the carrier. It is preferable to make noise measurements on equipment

under the same gating conditions that will be used in the radar system. Some devices, such as high power transmitters, cannot operate continuously and only gated noise measurements are possible. The gated phase noise spectrum is the summation of the CW phase noise spectrum replicas centered at frequencies $\pm nf_R$, where f_R is the PRF and n is an integer. The total gated phase noise in the PRF bandwidth f_R equals the total CW phase noise in the transmit pulse bandwidth. In terms of stability requirements, the system requirements are derived using gated phase noise, which in turn is converted to a CW value for specifying components such as oscillators. The CW phase noise floor is smaller by a factor of the ratio of the PRF to the transmit bandwidth when the CW phase noise is assumed to be white.

Sensitivity loss due to phase noise is quantified by the increase in the system noise floor in the "clutter-free" doppler filters due to the phase noise sidebands on a large signal such as main-beam clutter. Sensitivity loss is the amount by which the total noise (thermal plus phase) exceeds the thermal noise level, as shown in Eq. 4.8. A gated phase noise to thermal noise ratio of –4 dB results in an approximately 1.5 dB sensitivity loss. This assumes a worst-case scenario with the main-beam clutter return at the A/D saturation level. CAGC, discussed in Section 4.1, is typically used to regulate the mean clutter to a level below A/D saturation (typically by the amount of the expected clutter fluctuation level). With CAGC, sensitivity loss will be less than or equal to the calculated worst-case value.

$$[\text{Sensitivity Loss}]_{\text{dB}} = 10\log_{10}\left(1+\frac{\text{Gated Phase Noise Power Density}}{\text{Thermal Noise Power Density}}\right) \tag{4.8}$$

Table 4.5 contains a calculation of the phase noise floor requirements for an 180 kHz PRF waveform. Clutter levels that require a 12-bit (sign plus 11 amplitude bits) A/D converter are assumed, as shown in Figure 4.16. The transmit pulse duration is 1.75 μs, resulting in a transmit pulse bandwidth of approximately 0.5 MHz since no pulse compression is used. The rms thermal-noise power is the thermal-noise floor within the receive portion of IPP. This power level is given in decibels with respect to the carrier amplitude (dBc). The thermal-noise density is obtained by dividing this power by the PRF bandwidth. The maximum gated phase noise floor is set to be 4 dB below the thermal noise floor for at most a 1.5 dB sensitivity loss. The CW phase noise floor is then obtained by multiplying by the PRF to transmit bandwidth ratio.

TABLE 4.5 CW Phase Noise Density Floor Calculation

Parameter	Value [dB]	Units	Comment
Thermal Noise Power at A/D	–60.0	dBc	12-bit A/D (sign+11 bits) thermal noise set at 1.414 quanta
1/PRF Bandwidth	–52.6	dB/Hz	180 kHz PRF waveform
Thermal Noise Density Floor at A/D	**–112.6**	**dBc/Hz**	
Phase Noise to Thermal Noise Ratio	–4.0	dB	Margin for at most 1.5 dB sensitivity loss
Gated Phase Noise Density Floor	**–116.6**	**dBc/Hz**	
PRF-to-Transmit Bandwidth Ratio	–5.0	dB	0.5 MHz transmit pulse bandwidth 1.75 μs pulse width w/ no PC
CW Phase Noise Density Floor	**–121.6**	**dBc/Hz**	

TABLE 4.6 Notional Subsystem Phase Noise Allocation

Subsystem		Allocation Percentage	Allocation dB	Adjustment for Common Source [dB]	Requirement [dBc/Hz]
Transmitter		20.0%	−7.0	0.0	−128.6
Exciter	AM	12.5%	−9.0	0.0	−130.6
	PM	37.5%	−4.3	−3.0	−128.9
Reciver		20.0%	−7.0	0.0	−128.6
Synchronizer		10.0%	−10.0	−3.0	−134.6
System		**100.0%**			**−121.6**

The system-level CW phase noise floor requirement (−121.6 dBc/Hz) is allocated to the contributing hardware units. The percentages are based on experience and negotiations with the subsystem designers. A possible allocation is provided in Table 4.6.

Discretes. Some sources of discrete sidebands are ripple on power supplies and the pickup of digital clocks. It is desirable to keep the integrated discrete sidebands below noise at the CFAR input to prevent detecting these discretes and producing false alarms. All coherent and postdetection integration must be accounted for when we specify discrete phase noise requirements.

Common discretes are affected by the time-delay between the portion imparted on the transmit and that on receive. The time-delay changes the correlation between the phase of the spurious modulating frequency from the transmit path with the phase from the receive path.[54] This can relieve the common discrete level requirement for low-PRF (or MTI) waveforms that are range unambiguous. However, for highly range ambiguous medium-PRF and high-PRF waveforms, the assumption is made that the noise common to transmit and receive adds noncoherently in the downconversion process. As a result, the common discrete power increases by 3 dB.

Table 4.7 provides the calculation for the system requirements for independent and common discrete levels. As in Table 4.5, a maximum clutter level requiring a 12-bit A/D is assumed and the rms thermal-noise level at the A/D converter is set to 1.414 quanta. To form the doppler filters, 2048 pulses are coherently integrated.

TABLE 4.7 Discrete Level Requirement Calculation

Parameter		Value [dB]	Units	Comment
Thermal Noise Power at A/D		−60.0	dBc	12-bit A/D (sign+11 bits) thermal noise set at 1.414 quanta
Total Integration Gain	Number of Pulses Coherently Integrated	33.1	dB	2048 IPPs integrated per CPI
	Dopper Filter Weighting	−2.66	dB	90 dB Dolph-Chebyshev weighting loss
	Number of CPIs Noncoherently Integrated	3.82	dB	PDI of 3 CPIs per Look 10 $\log_{10}(N_{pdi}{}^{0.8})$
Thermal Noise Power at CFAR		−94.3	dBc	Effective noise level after integration
Discrete to Thermal Noise Margin		−4.0	dB	Provides low P_{FA} due to discretes
Independent Discrete Requirement		**−98.3**	**dBc**	
Common Discrete Requirement		**−101.3**	**dBc**	3 dB less than Independent Discrete

To reduce doppler filter sidelobes, a 90 dB Dolph-Chebyshev weighting is applied, which reduces the coherent integration SNR gain by about 2.66 dB. For detection, three CPIs are integrated noncoherently via PDI for an approximate integration gain in dB of $10 \log_{10}(N_{\text{PDI}}{}^{0.8})$, or 3.82 dB. This results in a thermal-noise level of –94.3 dBc at the detector. A discrete to thermal-noise margin of –4 dB is used to provide a low P_{FA} due to discretes. The common discrete requirement is made 3 dB more stringent relative to the independent requirement as discussed above.

4.4 RANGE AND DOPPLER AMBIGUITY RESOLUTON

Medium and high-medium PRF waveforms usually use multiple discrete PRF ranging to resolve range ambiguities, while linear FM ranging is commonly employed when high-PRF waveforms are used.

Multiple Discrete PRF Ranging. The techniques for calculating true range from several ambiguous measurements generally involve sequential measurement of the ambiguous range in each PRF, followed by an *unfolding* and correlation process. The unfolding creates a vector of possible ranges for each valid detection by adding a set of integers [0 … K] times the unambiguous range interval:

$$R_{\text{unfold}} = R_{\text{ambiguous}} + \frac{c}{2f_R}[0 \ldots K] \tag{4.9}$$

where the unambiguous range interval = $c/(2f_R)$, with c = speed of light and f_R = PRF. The set of integers [0…K] are referred to as the range ambiguity numbers, with K determined by the maximum range of interest (K = CEIL[$2R_{\max} f_R/c$]). Range correlation occurs when the unfolded detections are scanned and a correlation window is applied across looks, as shown in Figure 4.17. In this example, the correlated target range has an ambiguity number of 4 (5th time around echo) on PRF 1, and an ambiguity

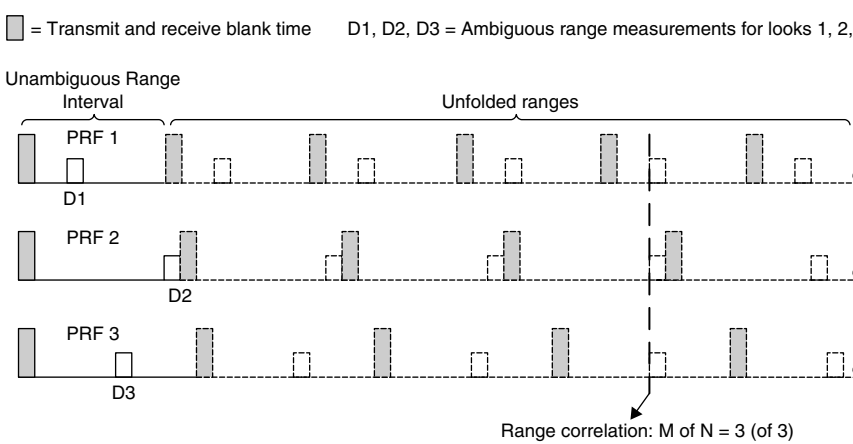

FIGURE 4.17 Range correlation example with 3 PRFs

number of 3 on PRFs 2 and 3. The IPP lengths (often expressed in *range gates per IPP*) are usually kept relatively prime (no common factors except the number 1) to permit unambiguous ranging at the maximum possible range.

The logic for correlation requires at least M detections across the N PRFs in a dwell to declare a target report (with M typically ≥ 3 for medium- and high-medium PRF waveforms). Range ghosts occur if the correlated range does not represent the true target range and typically occur when there is more than one detection per look. Range ghosts can also occur if a target detection on a single look correlated with other dissimilar target(s), or if multiple range correlations occurred on a set of detections corresponding to a single unique target (i.e., multiple unfolded ranges fell within the correlation window).

One method for efficiently scanning and correlating the unfolded detections involves *coarse binning,* as shown in Figure 4.18. Here, ambiguous detections are first amplitude centroided and then unfolded, as discussed previously, but with the results stored in an array whose elements are the coarse bins. These bins have a size less than or equal to the shortest IPP, and correlation involves scanning identical bins across all of the PRFs in the dwell and applying a correlation window. In the example shown in Figure 4.18, the bins are set to nine range gates (shortest IPP length), and the fifth coarse bin contains detections across the three PRFs that fall within the correlation window of ± 0.3 range gates. Blank, or empty, bins occur when the unfolded range falls outside a particular coarse bin interval. Key advantages to this approach are the ability to change the range correlation window dynamically and perform motion compensation easily for the range change across the dwell due to radar platform motion and/or the target's motion (if the unambiguous doppler has been resolved prior to this process). Additionally, the range gate sizes do not need to stay the same across the set of PRFs used in the dwell; in this case, the ambiguous range gate measurements on each look are first converted to common distance units (e.g., meters) prior to the unfolding and scanning/correlation processes.

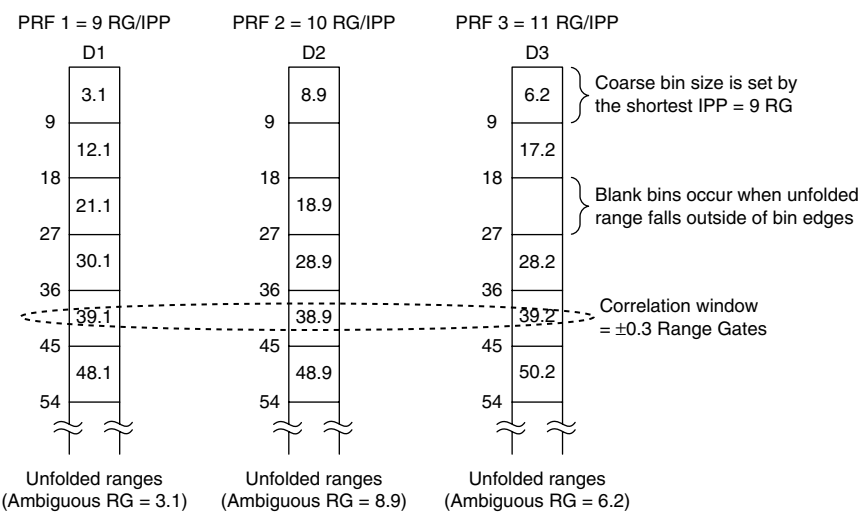

FIGURE 4.18 Range correlation using coarse binning on unfolded, centroided ambiguous detections. In this example, range gate size is the same for all three PRFs.

Additional criteria can be used to reject range ghosts, such as selecting the correlated range with the highest *M-of-N* value, selecting the detections based on the minimum variance across the *M* detections, or using maximum likelihood techniques.[55] The computed radar cross section (RCS) of correlations can also be used in the correlation process to reject sidelobe discrete detections as described in Section 4.2 (postdetection STC).

The ghosting problem can be mitigated further by a combination of doppler and/or monopulse binning. Resolving the doppler ambiguities first (prior to range correlation) will reduce the set of detections to those within the doppler correlation window. For cases where this is not feasible (generally the lower medium PRFs), utilizing both range and doppler correlation will reduce ghosts. Using monopulse measurements to segregate and bin targets that are distinguishable in angle can also reduce ghosting when there are a significant number of detections in a dwell.

A typical medium- or high-medium-PRF pulse doppler waveform cycles through *N* unique PRFs in a processing dwell (*N* typically being 5 to 8). The medium PRFs generally cover nearly an octave in frequency for good doppler visibility and ground moving target rejection. However, high-medium PRFs have inherently good doppler visibility (since they are ambiguous in sign only), so the span of the PRFs in a set of *N* PRFs is usually much less than an octave. Additional constraints on PRF selection for both waveforms include good visibility in sidelobe clutter (where some PRFs may be obscured by clutter in portions of the ambiguous range interval) and minimization of ghosts in the ambiguity resolution processing.

Doppler Ambiguity Resolution. Resolution of the unambiguous doppler-velocity is needed for medium-PRF waveforms, and it is generally done with a similar unfolding and correlation technique, as described previously for range ambiguities. As shown in Figure 4.19, velocity unfolding of detections involves adding a set of signed integers

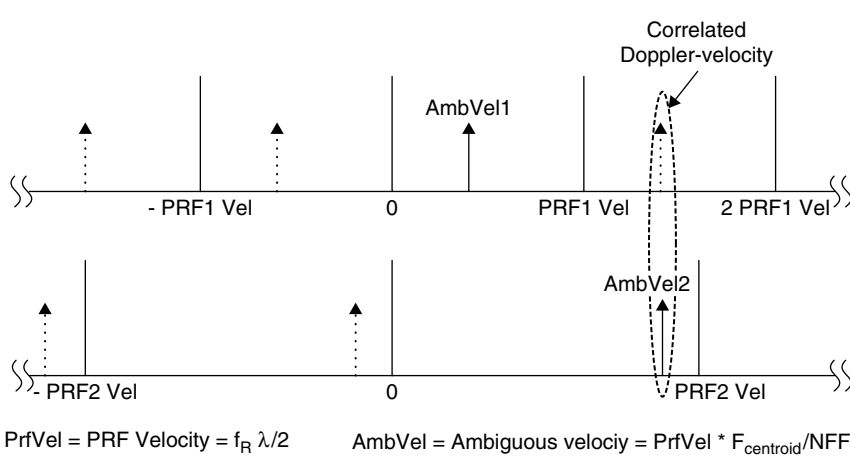

FIGURE 4.19 Doppler-velocity correlation performed on two detections across two looks. Ambiguous detections are unfolded out to a maximum positive and negative velocity.

times the PRF *velocity* (first blind speed) to each measured ambiguous radial velocity as follows:

$$V_{\text{unfold}} = \frac{f_R \lambda}{2}\left(\frac{F_{\text{centroid}}}{N_{\text{FFT}}} + [-J \ldots 0 \ldots K]\right) \tag{4.10}$$

where $f_R\lambda/2$ is the first blind speed (PRF velocity), F_{centroid} is the amplitude-centroided doppler filter number, N_{FFT} is the number of filters in the doppler filter bank, and $[-J \ldots 0 \ldots K]$ represents the set of doppler ambiguity numbers covering the maximum negative and positive doppler-velocities for the targets of interest. For cases where there are only a few ambiguities in doppler, doppler correlation may be performed prior to or in conjunction with range correlation to minimize ghosting.

High-PRF Ranging. Range-ambiguity resolution in high PRF is performed by modulating the transmitted signal and observing the phase shift of the modulation on the return echo. Modulation methods include varying the PRF, either continuously or in discrete steps; varying the RF carrier, with either linear or sinusoidal FM; or some form of pulse modulation such as pulse-width modulation (PWM), pulse-position modulation (PPM), or pulse-amplitude modulation (PAM). Of these modulation techniques, PWM and PPM may have large errors because of clipping of the received modulation by eclipsing or straddling (discussed in Section 4.6), and PAM is difficult to mechanize in both the transmitter and the receiver. Consequently, they will not be further considered here.

Linear-Carrier FM. Linear frequency modulation (FM) of the carrier can be used to measure range. The modulation and demodulation to obtain range are the same as used in frequency-modulated continuous-wave (FM-CW) radar,[56] but the transmission remains pulsed.

Suppose the dwell time is divided into two looks. In the first look, no FM is applied, and the doppler shift of the target is measured. In the second look, the transmitter frequency is varied linearly at a rate $\dot{f}$ in one direction (i.e., increasing or decreasing in frequency). During the roundtrip time to the target, the local oscillator has changed frequency so the target return has a frequency shift, in addition to the doppler shift, that is proportional to range. The difference in the frequency Δf of the target return between the two looks is found, and the target range calculated from

$$R = \left|\frac{c\Delta f}{2\dot{f}}\right| \tag{4.11}$$

The problem with only two FM segments during a dwell is that, with more than a single target in the antenna beamwidth, range ghosts result. For example, with two targets present at different dopplers, the two frequencies observed during the FM period cannot be unambiguously paired with the two frequencies observed during the no-FM period. To mitigate this problem, a three-segment scheme is used with the following segments: no-FM, FM-up, and FM-down. The range is found by selecting returns from each of the three segments that satisfy the relations

$$f_1 < f_0 < f_2 \tag{4.12}$$

$$f_1 + f_2 = 2f_0 \tag{4.13}$$

TABLE 4.8 Three-slope FM Ranging Example

There are two targets, *A* and *B;* FM slope = 24.28 MHz/s.

Target	***A***	***B***
Range (nmi)	10	20
Doppler frequency (kHz)	21	29
FM shift (kHz)	3	6
Observed Frequencies		
f_0, no FM (kHz)	21	29
f_1, FM up (kHz)	18	23
f_2, FM down (kHz)	24	35

Possible sets that satisfy the relations shown in Eq. 4.12 and Eq. 4.13 are

f_1	f_0	f_2	$2f_0$	$f_1 + f_2$	**Target?**	**Range (nmi)**
18	21	24	42	42	Yes	10
18	21	35	42	53	No	
18	29	35	58	53	No	
23	29	35	58	58	Yes	20

where f_0, f_1, and f_2 are the frequencies observed during the no-FM, FM-up, and FM-down segments, respectively. The range then is found from Eq. 4.11, where

$$\Delta f = f_2 - f_0 \quad \text{or} \quad (f_2 - f_1)/2 \quad \text{or} \quad f_0 - f_1 \tag{4.14}$$

An example is shown in Table 4.8.

If more than two targets are encountered during a dwell time, ghosts again result, as only $N - 1$ simultaneously detected targets can be resolved ghost-free where N is the number of FM slopes. However, this problem is not severe in practice, since multiple targets in a single beamwidth are usually a transient phenomenon.

The accuracy of the range measurement improves as the FM slope increases since the observed frequency differences can be more accurately measured. The FM slope is, however, limited by clutter-spreading considerations, since during the FM periods, the clutter is smeared in frequency and can appear in frequency regions normally clear of clutter.[57] A no-FM, FM-up, double FM-up scheme is recommended to prevent desired targets from competing with main-beam clutter. Range accuracies on the order of 1 or 2 miles can be reasonably achieved.

4.5 MODE AND WAVEFORM DESIGN

Modern multifunction pulse doppler radars utilize various modes to accomplish tasks such as search and track. Each mode uses certain waveforms optimized for the detection and measurement of various target characteristics.

For example, the radar operator might select a search mode and specify a search volume that the radar will raster scan, as shown in Figure 4.7. Valid detections in search are then converted to tracks in the radar computer. These tracks need to be updated by a track mode on a regular basis depending on the track accuracy required. High track accuracy is needed for threatening targets or those that need a fire control

solution in order to engage, as opposed to nonthreatening targets where a general situational awareness is sufficient and high accuracy is not required.

Search. The two primary search modes are *Autonomous Search* and *Cued Search*. In Autonomous Search the operator selects a range, azimuth, and elevation coverage, and the radar searches each beam position that covers this volume once per frame. The time it takes to complete a frame is known as the revisit or frame time. The *frame time* should be minimized to enhance the cumulative probability of detection of targets.

Modern radar systems can take advantage of on- and off-board cues to increase the probability of acquiring a target using Cued Search. A Cued Search mode adjusts the search volume and waveform selection according to the accuracy of the cue's parameters.

Radars with electronically scanned array (ESA) antennas can interleave other functions (track updates, Cued Search, calibrations, etc.) with Autonomous Search. The radar computer's resource manager must ensure that the maximum frame time is not exceeded with the inclusion of these other functions during a search frame.

For airborne pulse doppler radars, Autonomous Search can have two submodes: *Forward-aspect* and *All-aspect Search*. Forward-aspect Search is designed to detect head-on engagement targets with high closing speeds that are not competing against main-beam or sidelobe clutter. Forward-aspect Search uses high-duty high-PRF waveforms to maximize the energy on target and provide long detection range. Forward-aspect Search waveforms include *Velocity Search* (VS), *High-PRF Range-While-Search* (HRWS), and *Alert/Confirm*. All-aspect Search can be either a single high-medium PRF waveform that has acceptable performance for targets that are competing with sidelobe clutter, or the combination of Forward-aspect Search high-PRF waveforms interleaved with medium-PRF waveforms designed to detect targets competing with sidelobe clutter, such as *Medium-PRF Range While Search* (MRWS).

Velocity Search. VS is a high-PRF search waveform that measures doppler frequency unambiguously (with the possible exception of sense), but does not measure range. This is the classic high-PRF waveform. The transmit duty cycle is maximized to increase detection range. The receiver may be range gated to match the bandwidth of the transmit waveform, but range measurement is not attempted.

A VS dwell will consist of a single look at a given PRF. The coherent integration time is maximized within the limits of the maximum expected target radial acceleration. VS is optimized for Swerling I and III target amplitude fluctuation statistics and the cumulative probability of detection of incoming targets over several search frames.

High-PRF Range-While-Search. Like VS, HRWS is a high-PRF waveform. However, linear-carrier FM ranging is used to obtain a range measurement, as described in Section 4.4. This range measurement comes at the expense of frame time with the addition of various FM slopes for each dwell. The accuracy of this range measurement is dependent upon the linear FM ranging slopes.

Alert/Confirm. The beam agility of ESA-based radars allows the use of sequential detection techniques.[58] A simplification of such techniques is known as Alert/Confirm.[59,60] The goal of Alert/Confirm is to provide high sensitivity while managing false alarms and minimizing the search frame time. By transmitting a longer *Confirm* dwell for ranging only at beam positions where a shorter-dwell *Alert* has detected

targets, Alert/Confirm provides the range measurement of classic HRWS waveforms without the frame time expense of transmitting linear FM ranging dwells every beam position. The Confirm dwell can also be used to control false alarms, permitting the Alert dwell to be more sensitive than classic VS.

The Alert phase is used to search each beam position of the frame for the presence of a target. A VS waveform is used with a low detection threshold and a corresponding false alarm time on the order of a few seconds. The lower detection threshold increases sensitivity. When an Alert dwell declares a detection, a Confirm dwell is scheduled for that Alert dwell's beam position. If monopulse measurements are available on the Alert detection, the Confirm beam can be centered on the detection to decrease beam-shape loss. The Confirm dwell is typically a HRWS waveform and only examines doppler filters within a window centered about the filter of the Alert detection cue. The Confirm dwell must produce a detection corresponding to the Alert detection in order for a valid detection declaration. The Confirm dwell is used to manage false alerts and provide a range measurement for target detections. The Alert and Confirm detection thresholds are designed to achieve overall false alarm time equal to conventional search (one every few minutes). Along with using the same PRF in Alert and Confirm, the time between these dwells, or *latency*, should be minimized to prevent a valid Alert detection from being eclipsed during the Confirmation dwell.

Low-latency also allows the use of *Correlated* Alert/Confirm. Here, a Swerling I target RCS fluctuation model is assumed. This implies that when the same RF carrier frequency is used for Alert and Confirm, the target RCS will be relatively constant between the two dwells,[61] providing additional range enhancement in terms of the cumulative probability of detection.

Medium-PRF Range While Search. A medium-PRF waveform is used to detect targets competing with sidelobe clutter that would be undetectable in HRWS. MRWS allows the detection of nose aspect targets at wide scan angles that are crossing the radar line-of-sight, such that their low closing velocity places them in sidelobe clutter and tail aspect targets in lead pursuit engagements (an attack geometry where the nose of the attacking aircraft is pointed ahead of the target's present position). MRWS provides complete situational awareness (perception of the surrounding tactical environment), but does not have the maximum detection range provided by the higher duty cycle of HRWS for thermal noise-limited targets.

The MRWS waveform uses M-of-N detection processing; a typical waveform might be 3-of-7. Each MRWS dwell is made up of N looks each with a different PRF. Detection is required on at least M looks to resolve target range and range rate unambiguously. The detection thresholds are set to provide approximately one false alarm per minute.

The effectiveness of MRWS is dependent on the ability to detect targets at the required ranges while simultaneously rejecting discrete clutter detections. Low two-way antenna sidelobes along with the combination of techniques discussed in Section 4.2, such as guard channel blanking and postdetection STC, are used to mitigate sidelobe clutter discrete false alarms.

MRWS also uses pulse compression to decrease the amount of sidelobe clutter that targets must compete with. The lower PRF reduces eclipsing and the amount of clutter range-folding. Transmit carrier frequency diversity dwell-to-dwell forces Swerling I and III target fluctuation statistics and improves cumulative probability of detection performance. Frequency diversity look-to-look within a dwell produces Swerling II and IV statistics and is better suited for high single-scan probability of detection.

MRWS can also be implemented with a high-medium PRF, which is characterized by the waveform's doppler coverage being unambiguous in doppler magnitude, but not doppler sense, for the maximum target doppler of interest. The resulting single blind speed due to main-beam clutter permits as wide of a clutter rejection notch as required to reject main-beam clutter or ground moving targets and still not result in doppler blind speeds for targets of interest. *M*-of-*N* ranging provides better range measurement accuracy than linear FM ranging used in HRWS. The PRFs used in a dwell must be chosen to resolve the high number of range ambiguities within the instrumented range.

Track. Target tracking is done by making range, range rate, and azimuth and elevation angle measurements on targets. Range measurements are obtained using range gating and centroiding on the target return with range ambiguities being resolved within the tracker. Range rate (i.e., doppler) measurements are formed with a centroid on the target's doppler return in the filter bank. Angle measurements can be obtained using monopulse, sequential lobing, or conical scan, with monopulse being the prominent choice in modern radars. The tracker creates windows, or groups of contiguous range-doppler cells, around each of these measurements in order to associate detections with existing tracks. The tracker, usually implemented with a nine-state (position, velocity, and acceleration) Kalman filter, estimates target motion in an inertial coordinate system.

Multiple-Target Tracking (MTT) can be accomplished in several ways. One method (*Track-While-Scan,* or TWS) is to use the normal search mode with FM or multiple-PRF ranging and store the range, angle, and doppler of the reported detections in the radar computer. These detections are then used to form and update track files. The antenna scans in a normal search pattern, and a scan-to-scan correlation is made on the detections that update the track files. Although tracking accuracies are less than can be achieved in a dedicated single-target track, multiple targets can be tracked simultaneously over a large volume of space.

A second method of Multiple-Target Tracking, *Pause-While-Scan,* particularly applicable to ESA-based radars, is to scan in a normal search pattern, pause on each search detection, and enter a Single-Target Track mode for a brief period. The advantage is that the resulting range, angle, and doppler measurements are more accurate than those made with a scanning antenna, but the time to search a volume in space is increased.

Transition-to-Track, or Track Acquisition, is used to confirm search target detections and provide improved range accuracy when needed. If the target is successfully acquired, a track file in the radar computer is initiated. The Track Acquisition waveform's parameters depend upon the type of search waveform that produced the target detection. The Track Acquisition waveform's thresholds are set to reject false alarms and reduce the false track initiation rate to less than one per hour.

For Track Acquisition, a search detection from VS would require a HRWS waveform to obtain a range measurement. HRWS and Alert/Confirm waveforms are followed by range gated high-PRF dwells using *M*-on-*N* ranging to achieve the necessary range accuracy for single PRF track updates. The unambiguous HRWS range measurement of the search detection is used to help resolve the range ambiguity. For MRWS detections, another MRWS dwell is used for Track Acquisition. Once the track file is initiated, several rapid track updates are used to firmly establish the track.

When doing Single-Target Track updates, a single PRF waveform can be used. The range and/or doppler ambiguities are resolved in search and, if necessary, in the Transition-to-Track phase. By using the unambiguous range and velocity predictions

of the target provided by the tracker, a single PRF can be chosen such that range and doppler eclipsing is avoided with high probability. The length of the dwell is adapted to provide sufficient energy on target so that its return signal-to-noise ratio will provide the necessary measurement accuracies required by the tracker. This adaptive track update waveform allows the search revisit time to be maintained while tracking multiple targets.

4.6 RANGE PERFORMANCE

The radar range equation is used to determine the performance of pulse doppler radar. The radar range equation must include losses, both system and environmental, that will degrade the strength of return signals at the detector. Probability of detection (P_d) depends on target signal-to-noise ratio and probability of false alarm (P_{FA}), which itself is a function of waveform. The false alarm probability determines the detection threshold and is referenced to an individual range-doppler cell. This per-cell probability is derived from the specified false report time for the system.

Radar Range Equation. In the doppler region where the signal does not fall in clutter, performance is limited only by system noise. The signal-to-noise power ratio in the range-doppler cell at the detector prior to postdetection integration for a target at range R is given by

$$\text{SNR} = \left(\frac{R_o}{R}\right)^4 \tag{4.15}$$

$$R_o = \left(\frac{P_{av} G_T G_R \lambda^2 \sigma_T}{(4\pi)^3 k T_s B_n L_T}\right)^{1/4} \tag{4.16}$$

where R_o = range at which SNR is equal to 1
σ_T = target radar cross section
L_T = losses applicable to the target

The remaining terms are as defined following Eq. 4.2. The net loss L_T used to compute SNR for a target is generally higher than the net loss L_C used to compute CNR in Eq. 4.2. L_T includes losses, such as eclipsing and range gate straddle, doppler filter straddle, CFAR, and guard blanking, that are applicable to resolvable targets but not to distributed clutter.

The target SNR represents the envelope ($\sqrt{I^2 + Q^2}$ for a linear detector or $I^2 + Q^2$ for a square-law detector) of the target return compared to that of just noise. The envelope is measured after the entire coherent matched filter process (i.e., transmit pulse matched filter, pulse compression, and coherent doppler filtering). Therefore, SNR is associated with a single CPI.

Losses. Some of the losses inherent in, but not necessarily unique to, pulse doppler radars that employ digital signal processing are discussed below. Some of the losses may be incorporated into the other variables in the radar range equation. Care must be taken to account for all of the system losses while avoiding redundancies.

Most *front-end* losses are applicable to both targets and clutter. Losses applicable only to targets will be indicated.

RF Transmit Loss. This loss accounts for RF ohmic losses between the transmitter or RF power amplifier and the antenna radiator, which can include losses from connectors, circulators, and radiating elements.

Radome Loss. Most radars require a radome to protect the antenna from environmental elements and to conform to the platform's shape. Radomes will have a loss that may depend on the scan angle of the antenna. This loss must be accounted for on transmit and receive (i.e., a two-way loss).

Propagation Loss. Propagation through the atmosphere results in a loss, especially at higher radar carrier frequencies. This loss is a function of range, altitude, and weather. It is also a two-way loss. Propagation loss is more of a environmental loss than a system loss, but can be grouped with the other losses that make up net loss in the radar range equation.

Scan Loss. Broadside electronically scanned array antennas are subject to reduction in gain when the main beam is scanned off broadside. The projected area of the ESA aperture decreases as beam scans from broadside. Projected area drops as cosine of scan (cone) angle. Mutual coupling between radiating elements further reduces the effective area. Scan loss must be accounted for on transmit and receive.

Beamshape Loss. This target-specific loss accounts for the loss in gain when the target is not located at the peak of the beam. Beamshape loss is defined as the increase in the power or the SNR required to achieve the same probability of detection on a target spread uniformly over the specified beam coverage as would occur with a target at beam center. Beamshape loss is used primarily in search detection range performance calculations.

RF Receive Loss. This loss is similar to RF Transmit Loss except it accounts for ohmic losses from the antenna face to the first low-noise amplifier. This loss may be included in the receive system noise figure or system temperature value.

IF Matched Filter Loss. The matched filter for a pulse doppler waveform includes the analog IF matched filter in the receiver and any subsequent digital integration of A/D samples to match the duration of the transmit pulse. IF matched filter loss quantifies how well the analog IF matched filter compares to the ideal matched filter for that point in the reception chain.

Quantization Noise Loss. This loss is due to the noise added by the A/D conversion process and to truncation due to finite word lengths in the signal-processor that follow.[62] This loss can also be incorporated into the receiver noise figure value.

Pulse Compression Mismatch Loss. This is caused by the intentional mismatching of the pulse compression filter to reduce time (range) sidelobes.

Eclipsing and Range Gate Straddle Loss. The large amount of range ambiguity inherent in pulse doppler waveforms results in the possible eclipsing of target returns

when the receiver is blanked during pulse transmission. In a multiple range gate system, the returns may also straddle gates reducing the pulse matched filter output of a single gate. Because of eclipsing and range gate straddle, the value of R_o, given by Eq. 4.16, may fall anywhere between zero and a maximum value, depending on the exact location of the target return within the interpulse period.

Figure 4.20 illustrates the effect of eclipsing and range gate straddle on the output of the pulse matched filter over the IPP. Each range gate is assumed to be matched to the transmit pulse bandwidth, which for unmodulated pulses (i.e., no pulse compression modulation) is the inverse of the pulse duration. Therefore, referring to Figure 4.6, the gate width τ_g equals the transmitted pulse τ_t. In Figure 4.20, the IPP is $5\tau_g$. The plots on the left represent a range gate spacing of τ_s equal to τ_g. Range gate straddle loss can be reduced by the use of overlapping gates at the expense of extra hardware and processing. The rightmost plots represent the use of 50% range gate overlap ($\tau_s = \tau_g/2$). The maximum pulse matched filter output as a function of return delay is shown in terms of relative voltage and power. The "voltage" plot shows the cumulative effect of convolving the return pulse with the matched filter of each range gate. For a single range gate, this is simply the convolution of two rectangular pulses, which results in a triangular response. To compute loss, the matched filter output in terms of power (i.e., voltage squared) must be used.

When the PRF is high, so that many range ambiguities occur, the target range delay may be considered to be random from frame to frame, with a uniform distribution over the IPP. A measure of performance reduction due to eclipsing and range gate straddle is found by

1. Using the uneclipsed detection curve (P_d vs. S/N) for the waveform and selecting a particular SNR of interest S/N_0 along with its corresponding probability of detection $P_{d,0}$.
2. Reduce S/N_0 by a factor related to the relative output "power" of the matched filter as a function of ambiguous range within the IPP. (See the third row of plots in Figure 4.20.)
3. With the reduced SNR, determine the new P_d as a function of ambiguous range within the IPP from the uneclipsed detection curve.
4. Average these new P_d values across the IPP.

The result will be a new detection curve including the average effect of eclipsing and range gate straddle. For a fixed P_d, the difference in SNR between the uneclipsed and the eclipsed detection curves is the average eclipsing and range gate straddle loss. This difference represents the average increase in signal-to-noise ratio required to obtain the same probability of detection with eclipsing and straddle, as in the case where the transmit pulse is received by a matched gate with no straddle. Since the detection curve changes shape, the loss depends on the probability of detection selected, which is depicted in Figure 4.21. For accurate results, eclipsing and range gate straddle loss must be computed together.

A less accurate approximation compares the average signal-to-noise ratio over the interpulse period with the signal-to-noise ratio of the matched case. In the case of N continuous range gates spanning the duration of the IPP, each of which are matched to the transmit pulse width, the approximate average eclipsing and straddle loss is[63]

$$\text{approximate eclipsing and range gate straddle loss} = \frac{12N}{7N-6} \tag{4.17}$$

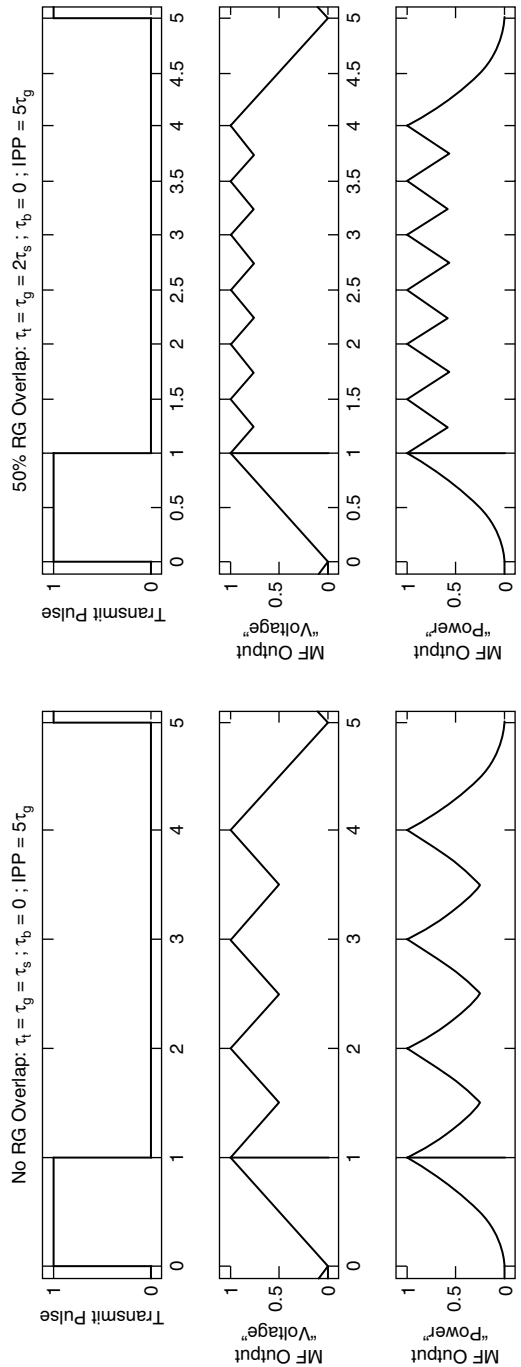

FIGURE 4.20 Concept of eclipsing and range gate straddle loss. The top row of plots shows the transmit pulse for a single IPP of a pulse doppler waveform with a duty cycle of 20%. The second row of plots shows the relative voltage of the maximum pulse matched filter (MF) output as a function of range-ambiguous target return within the IPP. The third row of plots shows the output in terms of relative power.

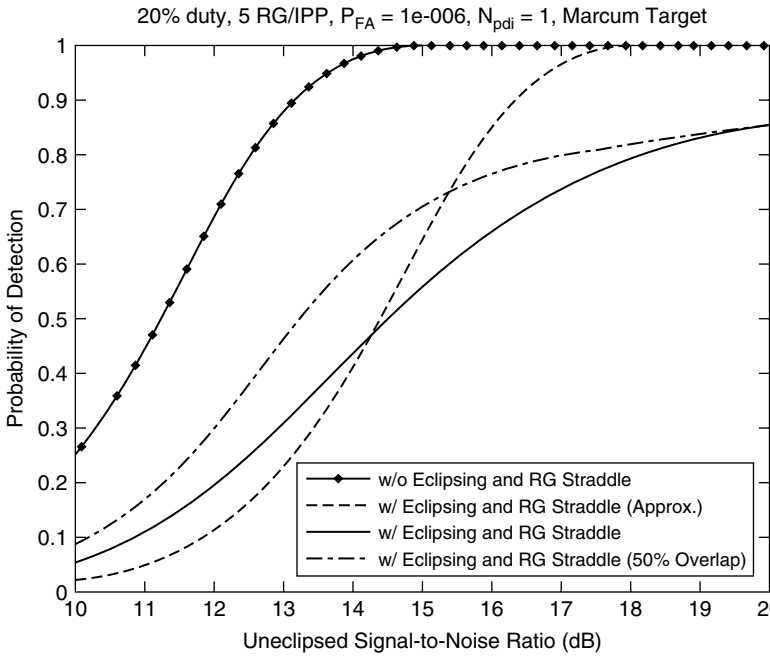

FIGURE 4.21 Comparison of detection performance with and without eclipsing and range gate straddle loss. The approximate performance using Eq. 4.17 is also provided. The performance with eclipsing and range gate straddle loss with the use of 50% overlapped range gates is shown.

Eq. 4.17 assumes an unmodulated, rectangular transmit pulse shape with the receive gate matched to the transmit pulse width. There is no range gate overlap. The first gate of the N range gates are blanked for the transmit pulse. As shown in Figure 4.21, this approximation is only valid for a P_d near 50%.

There are several other details that have not been included in Figure 4.21. As shown in Figure 4.6, a portion of the first valid receive range gate (and possibly a portion of the last range gate in the IPP) is typically blanked to avoid receiving transients of the transmit-to-receive (and receive-to-transmit) switching. Also, if pulse compression modulation is used on the transmit pulse, the range gate duration will be reduced to match the transmit pulse bandwidth. All of these effects should be included when computing the eclipsing and range gate straddle loss.

Doppler Filter Weighting Loss. This loss results from the increased noise bandwidth of the doppler filters that occurs because of filter sidelobe weighting. The loss can also be accounted for by an increase of the doppler filter noise bandwidth instead of as a separate loss.

Doppler Filter Straddle Loss. This loss is due to a target not always being in the center of a doppler filter. It is computed by assuming a uniformly distributed target doppler over one filter spacing and is a function of the doppler filter sidelobe weighting. This loss can be reduced (at the expense of increased processing) by zero-padding the collected data and performing a higher-point FFT to form highly overlapped doppler filters.

CFAR Loss. This loss is caused by an imperfect estimate of the detection threshold compared with the ideal threshold. The fluctuation in the estimate necessitates that the mean threshold be set higher than the ideal, hence a loss. It is only applicable to targets.

Guard Blanking Loss. This target-specific loss is the detectability loss in the main channel caused by spurious blanking from the guard channel. (See Figure 4.11.)

Probability of False Alarm. Radar detection performance is determined by the detection threshold, which in turn is set to provide a specified probability of false alarm.[64–68] As described in Section 4.4, pulse doppler radars often employ a multilook detection criterion to resolve range ambiguities. This can be accomplished with linear-FM ranging as in the HRWS waveform or *M*-of-*N* ranging used by MRWS. These ambiguity resolution techniques dictate how the probability of false alarm per range-doppler cell is computed. These calculations assume a noise-limited environment.

For HRWS, different linear-FM slopes are applied to looks 2 through *m* of a *m*-look dwell, where *m* is typically 3. The PRF is high enough for at most only a doppler sign ambiguity. Detections in looks 2 through *m*, must correlate in doppler with detections in the first look, which has no slope. A doppler correlation window is set equal to the maximum doppler offset due to linear-FM ranging from a target at the maximum instrumented range. For doppler-only correlation, the P_{FA} per range-doppler cell to provide a specified false report time is

$$P_{FA} = \frac{1}{N_r}\left(\frac{T_d \ln(2)}{\binom{m}{n} N_f N_{FM}^{m-1} T_{FR}}\right)^{1/m} \tag{4.18}$$

where N_r = number of independent range samples processed per IPP
N_f = number of independent doppler filters visible in the doppler passband (number of unblanked filters/FFT weighting factor)
T_d = total dwell time of the multiple PRFs including postdetection integration (if any), space change, and any dead time
n = number of looks in a dwell time
m = number of detections required for a target report (for a typical HRWS dwell, $n = 3$ and $m = 3$)
$\binom{m}{n}$ = binomial coefficient = $n!/[m!(n\text{-}m)!]$
T_{FR} = false-report time (per Marcum's definition where the probability is 0.5 that at least one false report will occur in the false-report time; this can be related to the average time T_{AVG} between false reports by $T_{FR} \approx T_{AVG} \ln(2)$)
$N_{FM} = k_{FM,max}(2R_{max}/c)$ = number of independent doppler filters in the doppler correlation window
$k_{FM,max}$ = steepest linear-FM slope magnitude
R_{max} = maximum instrumented range

Alert/Confirm increases sensitivity by allowing more false alarms in Alert and relying on Confirm to reject those false alerts. The Alert/Confirm combination is designed to provide the same false report time T_{FR} as a conventional waveform. A specified fractional increase F in frame time accounts for the execution of Confirm dwells to reject false Alert detections. F is on the order of 5–10%. When using a VS Alert and a 3-look HRWS Confirm, the probability of false alarm per range-doppler cell, $P_{FA,a}$ and $P_{FA,c}$ for Alert and Confirm, respectively, is

$$P_{FA,a} = \frac{T_{d,a}\ln(2)}{N_{r,a}N_{f,a}T_{FR,a}}$$
$$P_{FA,c} = \frac{1}{N_{r,c}}\left(\frac{2T_{d,c}\ln(2)}{N_{f,\text{cue}}N_{FM}^2 T_{FR}} \times \frac{F+1}{F}\right)^{1/3} \tag{4.19}$$

where $T_{d,a}$ = total Alert dwell time
$N_{r,a}$ = number of independent range samples processed per IPP in Alert
$N_{f,a}$ = number of independent doppler filters visible in the Alert doppler passband
$T_{FR,a}$ = $T_{d,c}/F$ = Alert false report time
$T_{d,c}$ = total Confirm dwell time
F = fractional increase in frame time allocated to Confirm (5–10%)
$N_{r,c}$ = number of independent range samples processed per IPP in Confirm
$N_{f,\text{cue}}$ = number of independent doppler filters in the Confirm window centered about the doppler of the Alert detection cue
N_{FM} = number of independent doppler filters in Confirm linear-FM ranging doppler correlation window
T_{FR} = overall Alert/Confirm false report time

The M-of-N ranging used in MRWS requires correlation in range and can be viewed as a binary detector. MRWS is typically a medium-PRF waveform with range and doppler ambiguities. Doppler is used for clutter mitigation in each look, and the doppler ambiguity may not need to be resolved since the tracker can determine range rate from successive dwells. A typical MRWS M-of-N correlation would be three detections out of eight looks (i.e., $m = 3$ and $n = 8$). For range-only correlation, the P_{FA} in each range-doppler cell is given by

$$P_{FA} = \frac{1}{N_f}\left[\frac{T_d\ln(2)}{\binom{m}{n}N_{ru}T_{FR}}\right]^{1/m} \tag{4.20}$$

where N_{ru} = number of independent range samples in the output unambiguous-range interval (display range/range gate size)

For better false alarm rejection, doppler correlation can be used for MRWS. In the case where both range and doppler correlation are used, the required P_{FA} is

$$P_{FA} = \left[\frac{T_d \ln(2)}{\binom{m}{n} N_{fu} N_{ru} T_{FR} W^{m-1}} \right]^{1/m} \tag{4.21}$$

where N_{fu} = number of independent doppler filters in the unambiguous doppler region
W = width (in doppler filters) of the correlation window applied to detections following initial detection

Probability of Detection. Using the P_{FA} per range-doppler cell, the probability of detection (P_d) of a given look can be determined for a given target SNR, the number of CPIs noncoherently integrated (N_{pdi}), and the target RCS fluctuation model assumed.[69] The inverse problem of determining the required SNR for a given P_d can be solved via approximations.[70] Universal detection equations have been published that provide reasonably accurate results and are reproduced here.[71] Again, the assumption that targets are in a gaussian noise-limited environment is made.

For a single look with N_{pdi} CPIs noncoherently integrated and a specified P_{FA} per range-doppler cell, the P_d as a function of SNR for a Marcum (nonfluctuating) target can be approximated as

$$P_d(\text{SNR}, P_{FA}, N_{pdi}) = \frac{1}{2} \text{erfc}\left(\sqrt{-0.8 \ln[4P_{FA}(1-P_{FA})]} + \sqrt{\frac{N_{pdi}}{2} - \frac{1}{2}} - \sqrt{N_{pdi}\ \text{SNR} + \frac{N_{pdi}}{2} - \frac{1}{2}} \right) \tag{4.22}$$

where erfc(·) is the complementary error function. The required SNR as a function of P_d for a Marcum target is approximated as

$$\text{SNR}_{reqd}(P_d, P_{FA}, N_{pdi}) = \frac{\eta^2}{N_{pdi}} + \frac{2\eta}{N_{pdi}} \sqrt{\frac{N_{pdi}}{2} - \frac{1}{4}} \tag{4.23}$$

where

$$\eta = \sqrt{-0.8 \ln[4P_{FA}(1-P_{FA})]} - \text{sign}(0.5 - P_d) \sqrt{-0.8 \ln[4P_d(1-P_d)]}$$

For Swerling fluctuating target models, the P_d and required SNR can be approximated, respectively, as

$$P_d(\text{SNR}, P_{FA}, N_{pdi}, n_e) = K_m \left[\frac{K_m^{-1}(P_{FA}, 2N_{pdi}) - 2(N_{pdi} - n_e)}{\frac{N_{pdi}}{n_e}\text{SNR} + 1}, 2n_e \right] \tag{4.24}$$

$$\text{SNR}(P_d, P_{FA}, N_{pdi}, n_e) = \left[\frac{K_m^{-1}(P_d, 2n_e) - 2(N_{pdi} - n_e)}{K_m^{-1}(P_d, 2n_e)} - 1 \right] \frac{n_e}{N_{pdi}} \tag{4.25}$$

where

$$n_e = \begin{cases} 1, & \text{for Swerling I target (chi-squared distribution with 2 degress of freedom)} \\ N_{\text{pdi}}, & \text{for Swerling II target (chi-squared distribution with } 2N_{\text{pdi}} \text{ degress of freedom)} \\ 2, & \text{for Swerling III target (chi-squared distribution with 4 degress of freedom)} \\ 2N_{\text{pdi}}, & \text{for Swerling IV target (chi-squared distribution with } 4N_{\text{pdi}} \text{ degress of freedom)} \end{cases}$$

$K_m(x,d) = 1 - P\left(\frac{d}{2}, \frac{x}{2}\right)$ = chi-squared distribution survival function[72]

$K_m^{-1}(p,d)$ = inverse chi-squared distribution survival function

$$P(\alpha,x) = \frac{\gamma(\alpha,x)}{\Gamma(\alpha)} = \frac{\int_0^x t^{\alpha-1}e^{-t}dt}{\int_0^\infty t^{\alpha-1}e^{-t}dt} = \text{regularized lower incomplete gamma function}$$

The integral of the chi-squared distribution $K_m(x,d)$ and its inverse $K_m^{-1}(p,d)$ are often included in mathematical computation software packages.[73]

When M-of-N detection (i.e., binary detection) is used within a dwell, the probability of detection for each look ($P_{d,\text{look}}$) is used to compute the probability of detection for a dwell ($P_{d,\text{dwell}}$). When a dwell requires m detections out of n looks for a target declaration, the $P_{d,\text{dwell}}$ is

$$P_{d,\text{dwell}} = \sum_{k=m}^{n} \binom{k}{n} P_{d,\text{look}}^k \, (1 - P_{d,\text{look}})^{n-k} \tag{4.26}$$

For Alert/Confirm detection performance, the P_d for the Alert dwell and the P_d for the Confirm dwell are individually computed as a function of SNR. Care must be taken to normalize the SNR to account for differences in doppler filter bandwidth between the Alert and Confirm waveforms. The multiplication of normalized probability of detection curve for the Alert dwell with that of the Confirm dwell results in an estimate of the composite P_d vs. S/N curve for Alert/Confirm. More accurate results must include the effects of latency between the Alert and Confirm dwells.

Search detection performance is often characterized by the cumulative probability of detection, $P_{d,\text{cum}}$, which is defined as the probability that the radar will detect a closing target at least once by the time the target has closed to a specified range. $P_{d,\text{cum}}$ is only defined for closing targets. The cumulative probability of detection for the kth scan, or frame, is

$$\begin{aligned} P_{d,\text{cum}}[k] &= 1 - \prod_{i=1}^{k} [1 - P_{d,\text{ss}}[i]] \\ &= P_{d,\text{cum}}[k-1] + P_{d,\text{ss}}[k]\,(1 - P_{d,\text{cum}}[k]) \end{aligned} \tag{4.27}$$

where $P_{d,\text{ss}}[k]$ is the single-scan probability of detection on the kth scan. The accumulation of single-scan probability of detections is started at a range where the target's $P_{d,\text{ss}}$ is approximately 5%. There is an optimal search frame time for cumulative detection performance. A balance must be achieved. A short frame time limits the amount of energy placed on target per dwell and lowers the single-scan P_d. A long frame time allows the target to close in range more between revisits, thus lowering the benefit of the accumulation. Figure 4.22 illustrates the difference between single-scan and cumulative probability of detection.

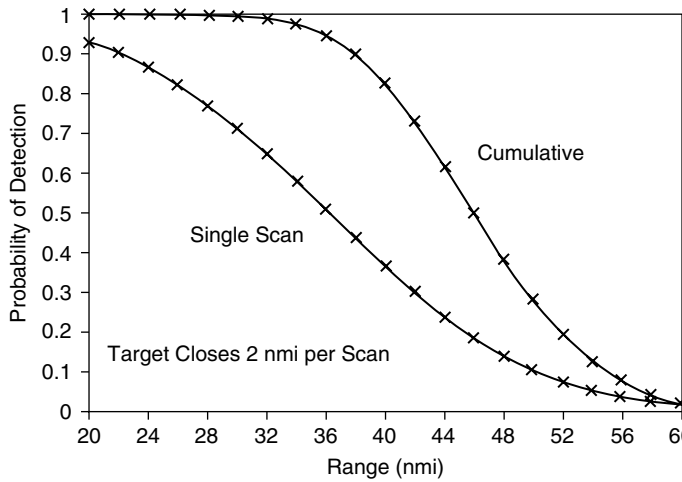

FIGURE 4.22 Single-scan vs. cumulative P_d as a function of range for a fixed radial-velocity moving target

Clutter-limited Case. The foregoing discussion assumed that the target fell in the noise-limited (i.e., clutter-free) part of the doppler band. If the target falls in the sidelobe clutter region, the range performance will be degraded, since the total interference power (system noise plus clutter) against which the target must compete is increased. The foregoing discussion can be applied to the sidelobe clutter region, however, by interpreting R_o as the range where the signal is equal to sidelobe clutter plus system noise.[74–76] The CFAR loss may also be higher owing to the increased variability of the threshold when the clutter varies over the target detection region. More accurate calculations of detection performance in the sidelobe clutter limited case should include the proper clutter RCS fluctuation models and CFAR techniques.[77]

LIST OF ABBREVIATIONS

AESA	active electronically scanned array
A/D	analog-to-digital
AGC	automatic gain control
AM	amplitude modulation
CAGC	clutter automatic gain control
CFAR	constant false alarm rate
CNR	clutter-to-noise power ratio
CPI	coherent processing interval
CW	continuous wave
Δ_{AZ}	delta-azimuth antenna beam (used for monopulse angle estimation)
Δ_{EL}	delta-elevation antenna beam (used for monopulse angle estimation)
dBc	decibels with respect to the carrier
DC	direct current
DFT	discrete Fourier transform

DPD	digital product detector
ESA	electronically scanned array
FFT	fast Fourier transform
FM	frequency modulation
FM-CW	frequency-modulated continuous-wave
HRWS	high-PRF range-while-search
I	inphase
IF	intermediate frequency
INS	inertial navigation system
IPP	interpulse period
LNA	low-noise amplifier
LO	local oscillator
MF	matched filter
MRWS	medium-PRF range-while-search
MTI	moving target indication
MTT	multiple-target tracking
NAGC	noise automatic gain control
PAM	pulse-amplitude modulation
P_d	probability of detection
PC	pulse compression
PDI	postdetection integration (noncoherent integration)
P_{FA}	probability of false alarm
PM	phase modulation
PPM	pulse-position modulation
PRF	pulse repetition frequency
PWM	pulse-width modulation
Q	quadrature
RCS	radar cross section
RFI	radio frequency interference
rms	root-mean-square
RF	radio frequency
R/P	receiver protector
RWS	range-while-search
Σ	sum receive antenna beam (primary beam used for detection)
SLB	sidelobe blanker
SNR	signal-to-noise power ratio
STC	sensitivity time control
TWS	track-while-scan
T/R	transmit/receive
VS	velocity search

REFERENCES

1. *IEEE Standard Radar Definitions,* IEEE Std 686–1997, 1997, p. 20.
2. D. C. Schleher, *MTI and Pulsed Doppler Radar,* Norwood, MA: Artech House, Inc., 1991, pp. ix–x.
3. F. E. Nathanson, *Radar Design Principles,* 2nd Ed. New York: McGraw-Hill, 1991, pp. 471–472.
4. M. I. Skolnik, *Introduction to Radar Systems,* Chapter 3, 3rd Ed. New York: McGraw-Hill, 2000.
5. G. W. Stimson, *Introduction to Airborne Radar,* Chapter 3 & Part X, 2nd Ed., Raleigh, NC: SciTech Publishing, Inc., 1998.

6. P. Lacomme, J. Hardange, J. Marchais, and E. Normant, *Air and Spaceborne Radar Systems: An Introduction.,* Chapter 2, Norwich, NY: William Andrew Publishing, LLC, 2001.
7. S. A. Hovanessian, *Radar System Design and Analysis*, Chapter 12, Norwood, MA: Artech House, Inc., 1984.
8. M. I. Skolnik, *Radar Applications*, New York: IEEE Press, 1988.
9. R. J. Doviak, D. S. Zrnic, and D. S. Sirmans, "Doppler weather radar," in *Proceedings of the IEEE,* vol. 67, no. 11, 1979, pp. 1522–1553.
10. P. Mahapatra, *Aviation Weather Surveillance Systems: Advanced Radar and Surface Sensors for Flight Safety and Air Traffic Management,* London, UK: The Institution of Electrical Engineers, 1999.
11. K. C. Overman, K. A. Leahy, T. W. Lawrence, and R. J. Fritsch, "The future of surface surveillance-revolutionizing the view of the battlefield," in *Record of the IEEE 2000 International Radar Conference,* May 7–12, 2000, pp. 1–6.
12. Defense Science Board, Future DoD Airborne High-Frequency Radar Needs/Resources, Office of the Under Secretary of Defense for Acquisition and Technology, Washington, DC, April 2001.
13. M. I. Skolnik, *Introduction to Radar Systems,* 3rd Ed. New York: McGraw-Hill, 2002, pp. 171–172.
14. G. W. Stimson, *Introduction to Airborne Radar,* 2nd Ed. Raleigh, NC: SciTech Publishing, Inc., 1998, pp. 329–333.
15. F. C. Williams and M. E. Radant, "Airborne radar and the three PRFs," *Microwave Journal*, July 1983 and reprinted in M. I. Skolnik, *Radar Applications.* New York: IEEE Press, 1988, pp. 272–276.
16. D. C. Schleher, *MTI and Pulsed Doppler Radar*, Artech House, Inc., 1991, pp. 59–73.
17. G. Morris and L. Harkness, *Airborne Pulsed Doppler Radar,* 2nd Ed. Norwood, MA: Artech House, Inc., 1996, p. 4.
18. W. H. Long and K. A. Harriger, "Medium PRF for the AN/APG-66 radar," in *Proceedings of the IEEE,* vol. 73, issue 2, February 1985, pp. 301–311.
19. B. Cantrell, "ADC spurious signal mitigation in radar by modifying the LO," in *Proceedings of the 2004 IEEE Radar Conference,* April 26–29, 2004, pp. 151–156.
20. H. Hommel and H. Feldle, "Current status of airborne active phased array (AESA) radar systems and future trends," in *2005 IEEE MTT-S International Microwave Symposium Digest,* June 12–17, 2005, pp. 1449–1452.
21. S. M. Sherman, *Monopulse Principles and Techniques*, Norwood, MA: Artech House, Inc., 1984.
22. L. E. Pellon, "A double Nyquist digital product detector for quadrature sampling," *IEEE Transactions on Signal Processing*, vol. 40, issue 7, pp. 1670–1681, July 1992.
23. G. Minkler, *CFAR: The Principles of Automatic Radar Detection in Clutter*, Baltimore, MD: Magellan Book Company, 1990.
24. R. Nitzberg, *Radar Signal Processing and Adaptive Systems,* Chapter 7, Norwood, MA: Artech House, Inc., 1999.
25. M. Weiss, "Analysis of some modified cell-averaging CFAR processors in multiple-target situations," *IEEE Transactions on Aerospace and Electronic Systems,* vol. AES-18, no.1, pp. 102–144, January 1982.
26. P. P. Gandhi and S. A. Kassam, "Analysis of CFAR processors in nonhomogeneous background," *IEEE Transactions on Aerospace and Electronic Systems,* vol. 24, no. 4, July 1988.
27. J. Farrell and R. Taylor, "Doppler radar clutter," *IEEE Transactions on Aeronautical & Navigational Electronics,* vol. ANE-11, pp. 162–172, September 1964 and reprinted in D. K. Barton, *CW and Doppler Radars,* Section VI-2, Vol. 7. Norwood, MA: Artech House, Inc., 1978, pp. 351–361.
28. L. Helgostam and B. Ronnerstam, "Ground clutter calculation for airborne doppler radar," *IEEE Transactions on Military Electronics,* vol. MIL-9, pp. 294–297, July–October 1965.

29. A. L. Friedlander and L. J. Greenstein, "A generalized clutter computation procedure for airborne pulse doppler radars," *IEEE Transactions on Aerospace and Electronic Systems,* vol. AES-6, pp. 51–61, January 1970 and reprinted in D. K. Barton, *CW and Doppler Radars,* Section VI-3, Vol. 7, Norwood, MA: Artech House, Inc., 1978, pp. 363–374.
30. M. B. Ringel, "An advanced computer calculation of ground clutter in an airborne pulse doppler radar," in *NAECON '77 Record,* pp. 921–928 and reprinted in D. K. Barton, *CW and Doppler Radars,* Section VI-4, Vol. 7. Norwood, MA: Artech House, Inc., 1978, pp. 375–382.
31. R. L. Mitchell, *Radar Signal Simulation,* Chapter 11, Norwood, MA: Artech House, Inc., 1976.
32. J. K. Jao and W. B. Goggins, "Efficient, closed-form computation of airborne pulse doppler clutter," in *Proceedings of the 1985 IEEE International Radar Conference,* Washington, DC, 1985, pp. 17–22.
33. W. A. Skillman, *SIGCLUT: Surface and Volumetric Clutter-to-Noise, Jammer and Target Signal-to-Noise Radar Calculation Software and User's Manual,* Norwood, MA: Artech House, Inc., 1987, pp. 1–4.
34. D. C. Schleher, *MTI and Doppler Radar,* Norwood, MA: Artech House, Inc., 1991, pp. 131–135.
35. F. J. Harris, "On the use of windows for harmonic analysis with the discrete Fourier transform," in *Proceedings of the IEEE,* vol. 66, no. 1, January 1978, pp. 51–83.
36. W. A. Skillman, *Radar Calculations Using the TI-59 Programmable Calculator,* Norwood, MA: Artech House, Inc., 1983, p. 308.
37. R. E. Ziemer and J. A. Ziegler, "MTI improvement factors for weighted DFTs," *IEEE Transactions on Aerospace and Electronic Systems,* vol. AES-16, pp. 393–397, May 1980.
38. H. R. Ward, "Doppler processor rejection of ambiguous clutter," *IEEE Transactions on Aerospace and Electronic Systems,* vol. AES-11, July 1975 and reprinted in D. K. Barton, *CW and Doppler Radars,* Section IV–11, Vol. 7. Norwood, MA: Artech House, Inc., 1978, pp. 299–301.
39. R. H. Fletcher and D. W. Burlage, "An initialization technique for improved MTI performance in phased array radar," in *Proceedings of the IEEE*, vol. 60, December 1972, pp. 1551–1552.
40. D. H. Harvey and T. L. Wood, "Design for sidelobe blanking systems," in *Proceedings of the 1980 IEEE International Radar Conference,* Washington, DC, 1980, pp. 410–416.
41. L. Maisel, "Performance of sidelobe blanking systems," *IEEE Transactions on Aerospace and Electronic Systems,* vol. AES-4, pp. 174–180, March 1968.
42. H. M. Finn, R. S. Johnson, and P. Z. Peebles, "Fluctuating target detection in clutter using sidelobe blanking logic," *IEEE Transactions on Aerospace and Electronic Systems,* vol. AES-7, pp. 147–159, May 1971.
43. A. Farina, *Antenna-based Signal Processing Techniques for Radar Systems*, Chapter 3, Norwood, MA: Artech House, Inc., 1992, pp. 59–93.
44. D. A. Shnidman and S. S. Toumodge, "Sidelobe blanking with integration and target fluctuation," *IEEE Transactions on Aerospace and Electronic Systems,* vol. 38, no. 3, pp. 1023–1037, July 2002.
45. D. H. Mooney, "Post Detection STC in a Medium PRF Pulse Doppler Radar," U.S. Patent 4,095,222, June 13, 1978.
46. F. E. Nathanson, *Radar Design Principles,* 2nd Ed. New York: McGraw-Hill, Inc., 1991, pp. 281–282.
47. J. B. Tsui, *Digital Techniques for Wideband Receivers,* 2nd Ed., Raleigh, NC: SciTech Publishing Company, 2004, pp. 163–166.
48. L. P. Goetz and W. A. Skillman, "Master oscillator requirements for coherent radar sets," in *IEEE-NASA Symposium on Short Term Frequency Stability,* NASA-SP-80, November 1964.
49. R. S. Raven, "Requirements for master oscillators for coherent radar," in *Proceedings of the IEEE,* vol. 54, February 1966, pp. 237–243 and reprinted in D. K. Barton, *CW and Doppler Radars,* Section V-I, Vol. 7, Artech House, Inc., Norwood, MA, 1978, pp. 317–323.
50. R. S. Raven, Correction to "Requirements for master oscillators for coherent radar," in *Proceedings of the IEEE,* vol. 55, issue 8, August 1967, p. 1425.

51. M. Gray, F. Hutchinson, D. Ridgely, F. Fruge, and D. Cooke, "Stability measurement problems and techniques for operational airborne pulse doppler radar," *IEEE Transactions on Aerospace and Electronic Systems,* vol. AES-5, pp. 632–637, July 1969.
52. A. E. Acker, "Eliminating transmitted clutter in doppler radar systems," *Microwave Journal,* vol. 18, pp. 47–50, November 1975 and reprinted in D. K. Barton, *CW and Doppler Radars,* Section V-3, Vol. 7. Norwood, MA: Artech House, Inc., 1978, pp. 331–336.
53. J. A. Scheer and J. L. Kurtz, *Coherent Radar Performance Estimation,* Norwood, MA: Artech House, Inc., 1993, pp. 158–159.
54. S. J. Goldman, *Phase Noise Analysis in Radar Systems Using Personal Computers,* Chapter 2, New York: John Wiley & Sons, Inc, 1989.
55. G. V. Trunk and M. W. Kim, "Ambiguity resolution of multiple targets using pulse-doppler waveforms," *IEEE Transactions on Aerospace and Electronic Systems,* vol. 30, no. 4, pp. 1130–1137, October 1994.
56. F. E. Nathanson, *Radar Design Principles,* 2nd Ed. New York: McGraw-Hill, Inc., 1991, pp. 449–452.
57. M. B. Ringel, "The effect of linear FM on the ground clutter in an airborne pulse doppler radar," in *NAECON '79 Record,* vol. 2, Dayton, OH, May 15–17, 1979, pp. 790–795.
58. F. E. Nathanson, *Radar Design Principles,* 2nd Ed. New York: McGraw-Hill, Inc., 1991, pp. 120–123.
59. G. W. Stimson, *Introduction to Airborne Radar,* 2nd Ed. Mendham, NJ: SciTech Publishing, Inc., 1998, pp. 506–507.
60. P. L. Bogler, *Radar Principles with Applications to Tracking Systems,* New York: John Wiley & Sons, Inc., 1990, pp. 262–266.
61. R. A. Dana and D. Moraitis, "Probability of detecting a Swerling I target on two correlated observations," *IEEE Transactions on Aerospace and Electronic Systems,* vol. AES-17, no. 5, pp. 727–730, September 1981.
62. R. E. Ziemer, T. Lewis, and L. Guthrie, "Degradation analysis of pulse doppler radars due to signal processing," in *NAECON 1977 Record,* pp. 938–945 and reprinted in D. K. Barton, *CW and Doppler Radars,* Section IV-12, Vol. 7, Norwood, MA: Artech House, Inc., 1978, pp. 303–312.
63. P. Lacomme, J. Hardange, J. Marchais, and E. Normant, *Air and Spaceborne Radar Systems: An Introduction,* Norwich, NY: William Andrew Publishing, LLC, 2001, pp. 150–151.
64. J. I. Marcum, "A statistical theory of target detection by pulsed radar," *IEEE Transactions on Information Theory,* vol. IT-6, pp. 59–267, April 1960.
65. P. Swerling, "Probability of detection for fluctuating targets," *IEEE Transactions on Information Theory,* vol. IT-6, pp. 269–308, April 1960.
66. L. F. Fehlner, "Target detection by a pulsed radar," Report TG 451, Johns Hopkins University, Applied Physics Laboratory, Laurel, MD, 2 July 1962.
67. D. P. Meyer and H. A. Mayer, *Radar Target Detection: Handbook of Theory and Practice.* New York: Academic Press, 1973.
68. J. V. DiFranco and W. L. Rubin, *Radar Detection,* Norwood, MA: Artech House, Inc., 1980.
69. J. V. DiFranco and W. L. Rubin, *Radar Detection,* Norwood, MA: Artech House, Inc., 1980, pp. 287–445.
70. D. A. Shnidman, "Determination of required SNR values," *IEEE Transactions on Aerospace and Electronic Systems,* vol. 38, no. 3, pp. 1059–1064, July 2002.
71. D. K. Barton, "Universal equations for radar target detection," *IEEE Transactions on Aerospace and Electronic Systems,* vol. 41, no. 3, pp. 1049–1052, July 2005.
72. M. Evans, N. Hastings, and B. Peacock, *Statistical Distributions,* 3rd Ed. New York, John Wiley & Sons, Inc., 2000, p. 13.
73. W. H. Press, S. A. Teukolsky, W. T. Vetterling, and B. P. Flannery, *Numerical Recipes in C: The Art of Scientific Computing,* 2nd Ed. Cambridge, UK: Cambridge University Press, 1992, pp. 213–222.

74. D. Mooney and G. Ralston, "Performance in clutter of airborne pulse MTI, CW doppler and pulse doppler radar," in *1961 IRE Convention Record*, vol. 9, part 5, 1961, pp. 55–62 and reprinted in D. K. Barton, *CW and Doppler Radars,* Section VI-1, Vol. 7. Norwood, MA: Artech House, Inc., 1978, pp. 343–350.
75. M. B. Ringel, "Detection range analysis of an airborne medium PRF radar," in *IEEE 1981 NAECON Record,* Dayton, OH, 1981, pp. 358–362.
76. P. E. Holbourn and A. M. Kinghorn, "Performance analysis of airborne pulse doppler radar," in *Proceedings of the 1985 IEEE International Radar Conference,* Washington, DC, 1985, pp. 12–16.
77. D. A. Shnidman, "Radar detection probabilities and their calculation," *IEEE Transactions on Aerospace and Electronic Systems*, vol. 31, no. 3, pp. 928–950, July 1995.